Extreme poverty renders Madagascar highly vulnerable to underreported extreme heat that would not have occurred without human-induced climate change

Authors

1. Izidine Pinto, *Royal Netherlands Meteorological Institute (KNMI), De Bilt, The Netherlands, University of Cape Town, Cape Town, South Africa*
2. Rondrotiana Barimalala, *Norwegian Research Center, Bjerknes Center for Climate Research, Norway*
3. Sjoukje Philip, *Royal Netherlands Meteorological Institute (KNMI), De Bilt, The Netherlands*
4. Mariam Zachariah, *Grantham Institute, Imperial College London, UK*
5. Sayanti Sengupta, *Red Cross Red Crescent Climate Centre, The Hague, the Netherlands*
6. Maja Vahlberg, *Red Cross Red Crescent Climate Centre, The Hague, the Netherlands*
7. Emmanuel Raju, *Department of Public Health, Global Health Section & Copenhagen Centre for Disaster, Copenhagen, Denmark; African Centre for Disaster Studies, North-West University, Potchefstroom, South Africa*
8. Nick Baumgart, *Red Cross Red Crescent Climate Centre, The Hague, the Netherlands; Anticipation Hub, Berlin, Germany; Department of Public Health, Global Health Section & Copenhagen Centre for Disaster, Copenhagen, Denmark*
9. Carolina Pereira Marghidan, *Red Cross Red Crescent Climate Centre, The Hague, the Netherlands; Royal Netherlands Meteorological Institute (KNMI), De Bilt, The Netherlands; Faculty of Geo-Information Science and Earth Observation (ITC), University of Twente, Enschede, the Netherlands*
10. Clair Barnes, *Grantham Institute, Imperial College London, UK*
11. Joyce Kimutai, *Grantham Institute, Imperial College London, UK*
12. Piotr Wolski, *Climate System Analysis Group, University of Cape Town, Cape Town, South Africa*
13. Friederike E L Otto, *Grantham Institute, Imperial College London, UK*

Review authors

1. Roop Singh, *Red Cross Red Crescent Climate Centre, The Hague, the Netherlands*
2. Julie Arrighi, *Red Cross Red Crescent Climate Centre, The Hague, the Netherlands; Global Disaster Preparedness Center, Washington DC, USA; University of Twente, The Netherlands*
3. Christopher Jack, *Red Cross Red Crescent Climate Centre, The Hague, the Netherlands; Climate System Analysis Group, University of Cape Town, Cape Town, South Africa.*
4. Sarah Kew, *Royal Netherlands Meteorological Institute (KNMI), De Bilt, The Netherlands*
5. Ben Clarke, *Grantham Institute, Imperial College London, UK*

Main findings

- Heat waves in all regions of sub-saharan Africa are dramatically underreported leading to little awareness about the dangers of extreme heat. Heat-related mortality is estimated to increase by a factor of four by 2080, unless required investments to adaptation are made.
- South Madagascar is particularly vulnerable to impacts of heat waves, as food and agricultural systems are likely to collapse under high temperatures and compounding drought conditions and frequent, highly destructive cyclones. Extremely dry air during heat waves, including the nights, results in difficulty to breathe, and children are reported to be the worst affected with an overall high heat-related mortality.

- Using gridded observational products the very warm October is approximately a 1 in 100 year event in today's climate, while the extreme warm 7-day maximum and minimum temperatures are less rare, estimated to be a 1 in 25 and 1 in 20 year event respectively.
- To estimate the influence of human-caused climate change on this extreme heat we use a combination of climate models and the observations. We find that because of human-induced climate change the event would have been approximately 1 to 2 °C cooler for all three event definitions had humans not warmed the planet by burning fossil fuels.
- Due to the strong trend the change in likelihood is very large: it has increased by at least 100 times for October mean and 7-day minimum temperatures and by at least 10 times for the 7-day maximum temperatures.
- Unless the world rapidly stops burning fossil fuels, these events will become more common in the future. In a world 2°C warmer than preindustrial, events like these would no longer be rare but occur up to 3 times per decade.
- In Madagascar, less than half of the population has access to electricity and clean water, making most common coping strategies in extreme heat inaccessible to a large part of the population. Linked to the lack of clean water is one of the lowest child survival rates in the world. With very young children being particularly vulnerable to extreme heat these young lives are even more endangered.
- A high degree of informal settlements and unplanned urbanisation have resulted in large parts of the population particularly vulnerable to heat exposure. Factors like urban poverty, large workforce in informal economies, and loss of productivity/income during hot days result in compounding vulnerabilities.
- There are no heat action plans, early actions protocols, or comprehensive early warning systems, indicating an overall limited preparedness for heat waves. Investments in extreme heat forecasting, warning, and response capabilities are the most urgent requirements for Madagascar to better adapt to a warming world.

1 Introduction

Global mean surface air temperature (GSAT) has increased by 1.09ºC above pre-industrial levels during 2011-2020 and over the last 50 years it has increased at a rate unprecedented in at least the last 2000 years (Gulev et al., 2021). Increases in GSAT is a fingerprint of global warming and these increases represent a threat multiplier to society (e.g. Thompson et al 2023). Extended periods of high temperatures or heat waves can profoundly affect society and lead to an increase in heat-related fatalities. The number of people exposed to heat waves between 2000 and 2016 increased by around 125 million (WHO, 2018).

Madagascar is generally characterized by two main seasons, the warm and wet period taking place from October to April and the cold and dry season from May to September (Figure 1a). However, the spatial distribution of the mean temperature over the island is highly determined by the topography of the area. The north-south oriented mountain chain, reaching over 2000m in places, runs down the length of the country and creates distinct climatic regions. Specifically, the central and eastern parts (highlands) of the country have a mean annual temperature ranging from 15-23°C, while the temperature reaches above 25°C in the low-land western coasts (Figure S1). In terms of temperature, the difference between the two seasons is more defined over the highlands with the months of April and October usually considered as transition months. Due to the overall mild temperature and

favourable rainfall in the highlands, most agricultural activities occur in these areas, which are also the most densely populated parts of the country.

From July 2023 onwards, Madagascar experienced monthly average temperatures exceeding those recorded in any year since 1950. The temperature anomaly for October reached 1.64°C above the average (see figure 1a), with specific regions in the country exceeding 2.5°C (see figure 1b), putting residents and ecosystems under pressure, raising concerns about the health of citizens, and with potential repercussions on the country's agriculture and biodiversity (Fleuria, 2023). Consequently, October 2023 stands out as the warmest month in Madagascar since the 1950s (see figure 1c). Similar temperature conditions were seen in Madagascar during another episode of intense heat waves in 2019 (Météo Madagascar, 2019) which were extremely impactful on children, with consequences such as malnutrition, diarrhea and dehydration (Linfo.re, 2019). Persistent extreme weather occurrences, impacts from the COVID-19 pandemic paired with profound multidimensional poverty and structural vulnerabilities in agriculture, all contribute to the dysfunctionality of Madagascar's food supply chain. Elevated temperatures in Madagascar lead to a decline in labor productivity due to the impact of extreme heat.

According to the Climate Service Centre of the Southern Africa Development Communities (SADC-CSC, 2023), most of Madagascar experienced heat waves during October. In some parts, more than 10 days of heat wave conditions were recorded (Figure 2). The impacts of climate change, leading to drier conditions, have previously triggered extensive bushfires across Madagascar (e.g. in 2021) (Mongabay, 2023). Inhabitants in the southern and southwestern regions of the island are facing escalating challenges with worsening drought and famine (Hending and Holdereid, 2023).

Throughout 2023, global temperatures have been exceptionally warm, intensifying heat events across various land regions worldwide, including South America (Kew et al., 2023), North America, Europe, and China (Zachariah et al., 2023), as well as Morocco and Algeria (Philip et al., 2023).

We evaluate the degree to which human-induced climate change has influenced the occurrence of exceptionally high temperatures in October. The heat in Madagascar was early in the warm season, long-lasting and widespread. For this study we use three different event definitions to analyze the heat. The first is the average over October mean temperatures over all of Madagascar -Tmean (figure 1a). For the second and third definition we use a more local measure, to cover the impact on the more densely populated capital Antananarivo. For the local event definition we use the October maximum of 7-day mean maximum (TX7x) and October maximum of 7-day mean minimum temperature (TN7n). Including minimum temperature in the event definition is critical as a lack of relief from heat exposure at night markedly increases mortality risk compared to hot days followed by cool nights (see e.g. He et al., 2022; Murage et al., 2017; Kim et al., 2023; Royé, 2017).

Figure 3 illustrates this 7-day measure for 2023, which is 10th to 16th October 2023 for TX7x and 13th to 19th October 2023 for TN7n.
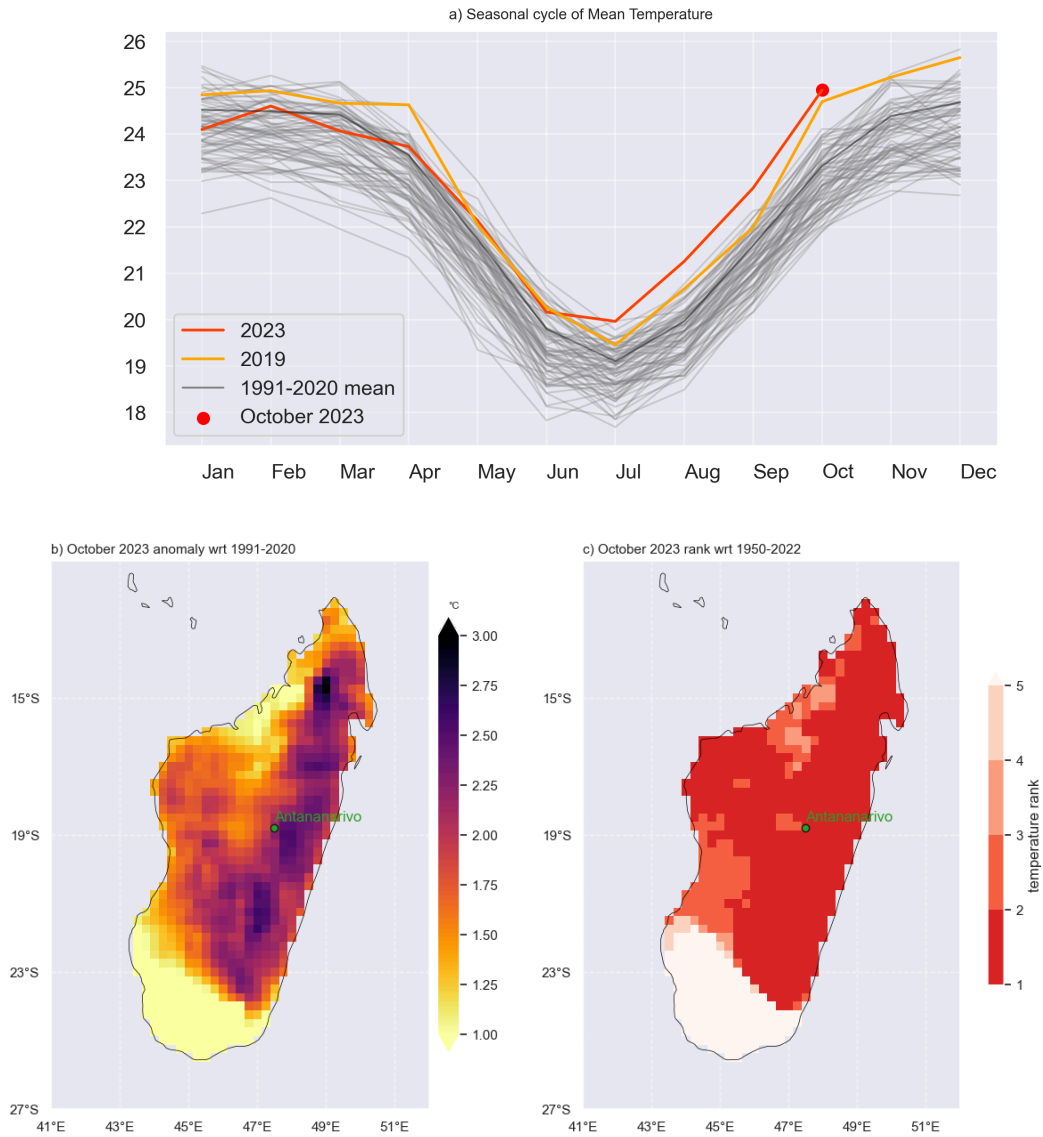
Figure 1: *Seasonal cycle of mean temperature over Madagascar from 1950-2023 (a), October 2023 mean temperature anomaly (b) and rank of October 2023 mean temperature (c). The densely populated capital Antananarivo is shown with a green circle. Data source: ERA5.*
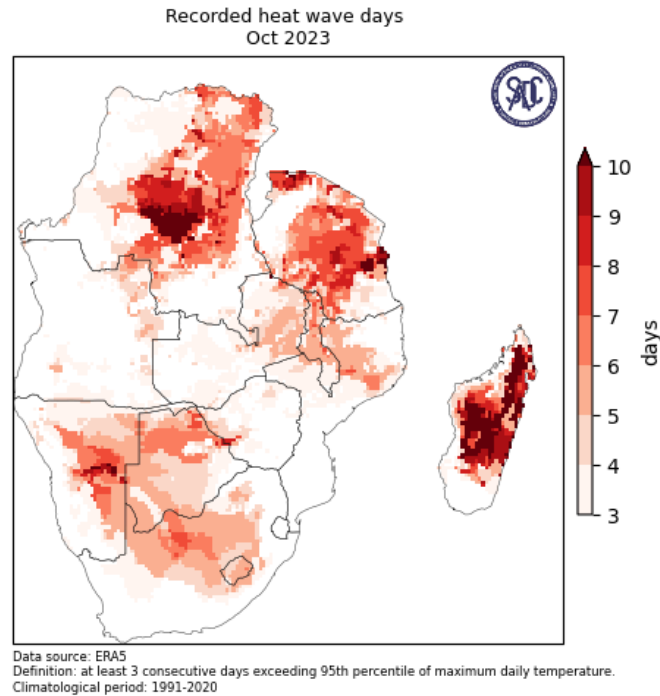
Figure 2: *Heat wave occurrence in October 2023 in the SADC region, based on ERA5 data, reported by the SADC Climate Services Centre in the [monthly monitoring bulletin](#).*
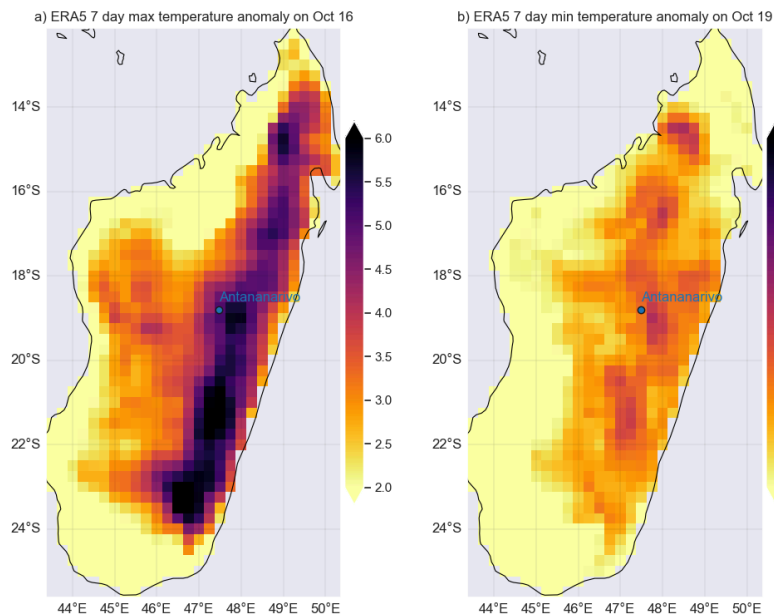

Figure 3: *ERA5 7 day average anomaly of daily maximum temperature (TX7x) for the period of 10th to 16th October 2023 (a) and 7 day average anomaly of daily minimum temperature (TN7x) for the period of 13th to 19th October 2023. Anomalies w.r.t. 1991-2020.*

To date, there have been limited attribution studies examining individual weather events in Madagascar, apart from the 2019-2021 meteorological drought in the southern part of the country ([Harrington et al., 2022](#)) and the 2022 rainfall from cyclone Batsirai ([Otto et al 2022](#)). Individual extreme temperature events remain significantly understudied and have attracted little attention until

October 2023 when the highland areas experienced relatively higher temperatures than the mean value. The Sixth Assessment Report (AR6) from the Intergovernmental Panel on Climate Change (IPCC) states that it is virtually certain that hot extreme events are increasing and this can be attributed to human activity (IPCC 2021; Seneviratne et al., 2021). Several land regions in Africa have experienced a discernible upward trend in mean, maximum and minimum temperatures (Gutiérrez et al., 2021) and there is a high level of confidence that these changes are primarily driven by human-induced climate change (Seneviratne et al. 2021, Fig SPM.3).

Using data from meteorological stations, Vincent et al., (2011) showed a significant increase in both mean and extreme temperature over Madagascar from 1961-2008. These results are then confirmed by Randriamarolaza et al., (2021), in which a significant increase in the daily mean and maximum temperatures were observed over the island by using station data from 1950-2018. The IPCC, AR6 assessed with high confidence that the mean temperature has increased in Madagascar, and with medium confidence on the increase in warm extremes (Seneviratne et al., 2021). The report further assessed a low confidence in attributing the increase in extremes to human activities. However, a recent detection and attribution analysis, using station data with output from the CMIP6 models, shows an increase in the intensity and frequency of extreme temperature in the region, mainly attributed to greenhouse gases and anthropogenic forcings (Randriamarolaza et al., 2023).

An investigation of the future changes in the frequency of heat wave events over Madagascar, using different climate model experiments and scenarios from CORDEX-CORE, CMIP5 and CMIP6 was performed by Coppola et al., (2021). They show that towards the end of the century, an increase of 4 to 6 heat wave events per year is projected in the region, with a strong agreement in all models. Heat wave events were defined as periods of more than 5 consecutive days during which the daily maximum temperature exceeds the control period (1970-2000) mean maximum temperature by at least 5C. Barimalala et al., (2021) also conducted a comprehensive analysis of the projected changes under 1.5 and 2 degrees global warming level (GWL) using the CORDEX-Africa outputs. Robust increases in both mean temperature and number of heat wave days per year were projected for most areas of the country. The IPCC AR6 further confirms with high confidence that Madagascar will very likely experience an increase in hot extremes at 1.5 degree GWL, while such an increase will be virtually certain at 4 GWL.

2 Data and methods

2.1 Observational data

We use the daily maximum temperatures (Tmax), daily minimum temperatures (Tmin) and monthly mean temperatures (Tmean) over a grid point close to the capital city Antananarivo and over the whole of Madagascar. The data is from the European Centre for Medium-Range Weather Forecasts (ECMWF) ERA5 reanalysis product (Hersbach et al., 2020). It should be noted that the variables from ERA5 are not directly assimilated, but these are generated by atmospheric components of the Integrated Forecast System (IFS) modelling system. The reanalysis begins in 1950, with data available until the end of the preceding month (October 2023).

Based on these data, SADC Climate Services Centre reported in their monthly monitoring bulletin that central and north-eastern Madagascar has experienced 7 or more days of heat waves in October 2023 (Fig. 3).

As a measure of anthropogenic climate change we use the (low-pass filtered) global mean surface temperature (GMST) taken from the National Aeronautics and Space Administration (NASA) Goddard Institute for Space Science (GISS) surface temperature analysis (GISTEMP, Hansen et al., 2010 and Lenssen et al. 2019).

2.2 Model and experiment descriptions

We use two multi-model ensembles from climate modelling experiments using different framings (Philip et al., 2020): regional climate models and coupled global circulation models.

1. Coordinated Regional Climate Downscaling Experiment CORDEX-AFRICA (10 models at 0.44° resolution (AFR-44) multi-model ensemble (Gutowski et al., 2016;), comprising 10 simulations resulting from pairings of Global Climate Models (GCMs) and Regional Climate Models (RCMs)). These simulations are composed of historical simulations up to 2005, and extended to the year 2100 using the RCP8.5 scenario.

2. CMIP6. This consists of simulations from 20 participating models with varying resolutions. For more details on CMIP6, please see Eyring et al., (2016). For all simulations, the period 1850 to 2015 is based on historical simulations, while the SSP5-8.5 scenario is used for the remainder of the 21st century.

2.3 Statistical methods

In this study we analyse time series of October mean temperature averaged over Madagascar, and daily October Tmin and Tmax at the grid point closest to Antananarivo, using data sets where long records of observed and modelled data are available. Methods for observational and model analysis and for model evaluation and synthesis are used according to the World Weather Attribution Protocol, described in Philip et al. (2020), with supporting details found in van Oldenborgh et al. (2021), Ciavarella et al. (2021) and here.

The analysis steps include: (i) trend calculation from observations; (ii) model evaluation; (iii) multi-method multi-model attribution and (iv) synthesis of the attribution statement.
We calculate the return periods, Probability Ratio (PR; the factor-change in the event's probability) and change in intensity of the event under study in order to compare the climate of now and the climate of the past, defined respectively by the GMST values of now and of the preindustrial past (1850-1900, based on the Global Warming Index). To statistically model the event under study, we use a Gaussian distribution that shifts with GMST for the October mean temperature and a GEV distribution that shifts with GMST for TX7x and TN7x. Next, results from observations and models that pass the evaluation tests are synthesised into single attribution statements.

3 Observational analysis: return period and trend

3.1 Analysis of gridded data

Using the ERA5 data, we calculate the return period, change in intensity and probability ratio between 2023 and a past climate that is 1.2°C cooler than now, for the October Tmean averaged over

Madagascar, the October TX7x over the grid box encompassing Antananarivo and the October TN7x over the grid box encompassing Antananarivo. The time series are shown in Figure 3, and the nonstationary linear models in Figure 4. We note that in both Tmean and, to a lesser extent, TX7x (Figure 4 a,b), there are far more high temperatures than are predicted by the model at the left-hand end of the plot, roughly corresponding to the years between 1950 and 1970: these are the points that lie above the fitted curve in Figure 4d. Although the linear model captures the trend in recent decades relatively well, it is unclear whether the poor fit in the early part of the time series is due to genuine nonlinearity or a change in the reliability of the ERA5 dataset prior to 1980. However, all of the observed values lie within the 95% confidence interval estimated from the linear model, and so we proceed with the analysis as usual, albeit with a caveat that trends extrapolated from the model are known to be uncertain. Due to this additional uncertainty, and also due to the extremity of the event, and the large estimated trend, the probability ratios between the 1.2 ℃ cooler climate and 2023 are not well defined. Therefore confidence is greater in values on intensity change, although we also report the probability ratios. Results are shown in Figure 4.

For October Tmean over Madagascar the return period is 106 years (28.3 to 1097 years). For the model analysis we use a rounded value of 100 years. The change in intensity is 1.424 ℃ (0.931 to 1.891 ℃). The probability ratio is 44029 (681 to 5.03E+07).

For October TX7x over Antananarivo the return period is 26.4 years (10.3 to 808 years). For the model analysis we use a rounded value of 25 years. The change in intensity is 1.953 ℃ (0.875 to 3.05 ℃). The probability ratio is 195 (at least 4.49).
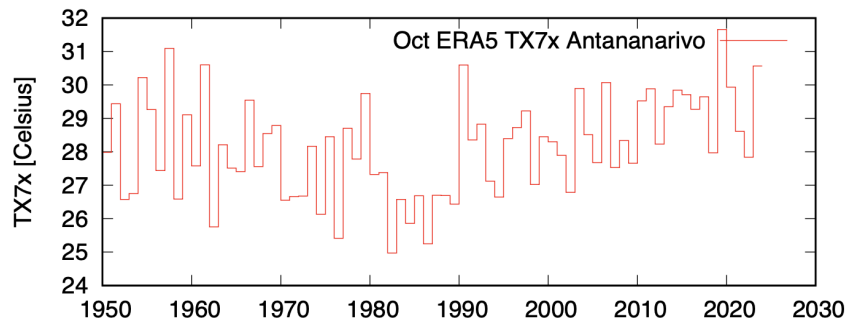
For October TN7x over Antananarivo the return period is 20.8 years (8.4 to 147 years). For the model analysis we use a rounded value of 20 years. The change in intensity is 1.784 ℃ (1.104 to 2.38 ℃). The probability ratio is at least 12.46.
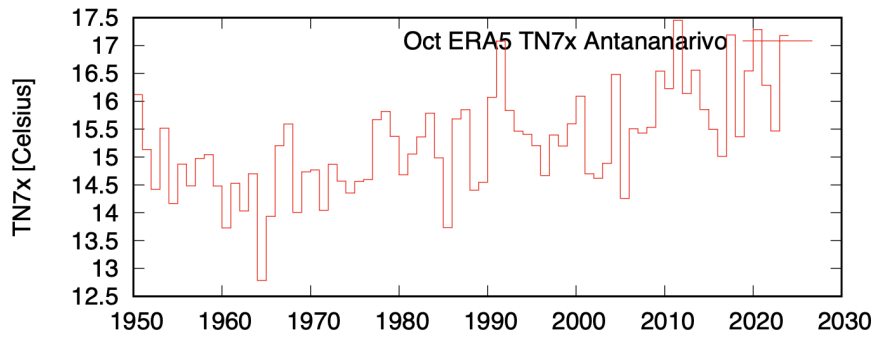
a)
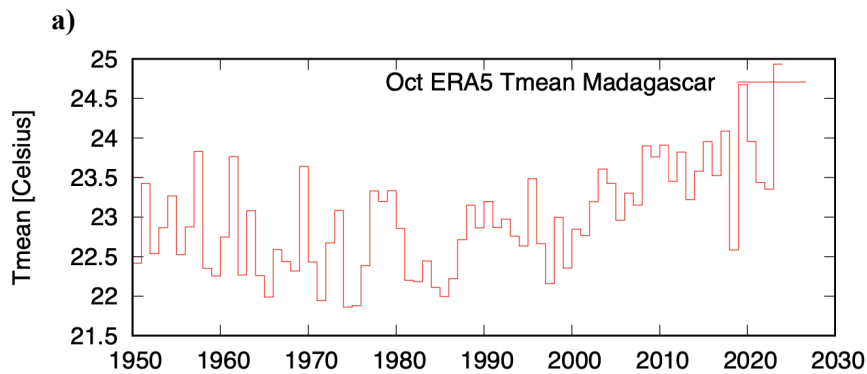
b)

c)

Figure 3: *Time series of the three event definitions: October Tmean over Madagascar (a), TX7x over Antananarivo (b) and TN7x over Antananarivo (c).*
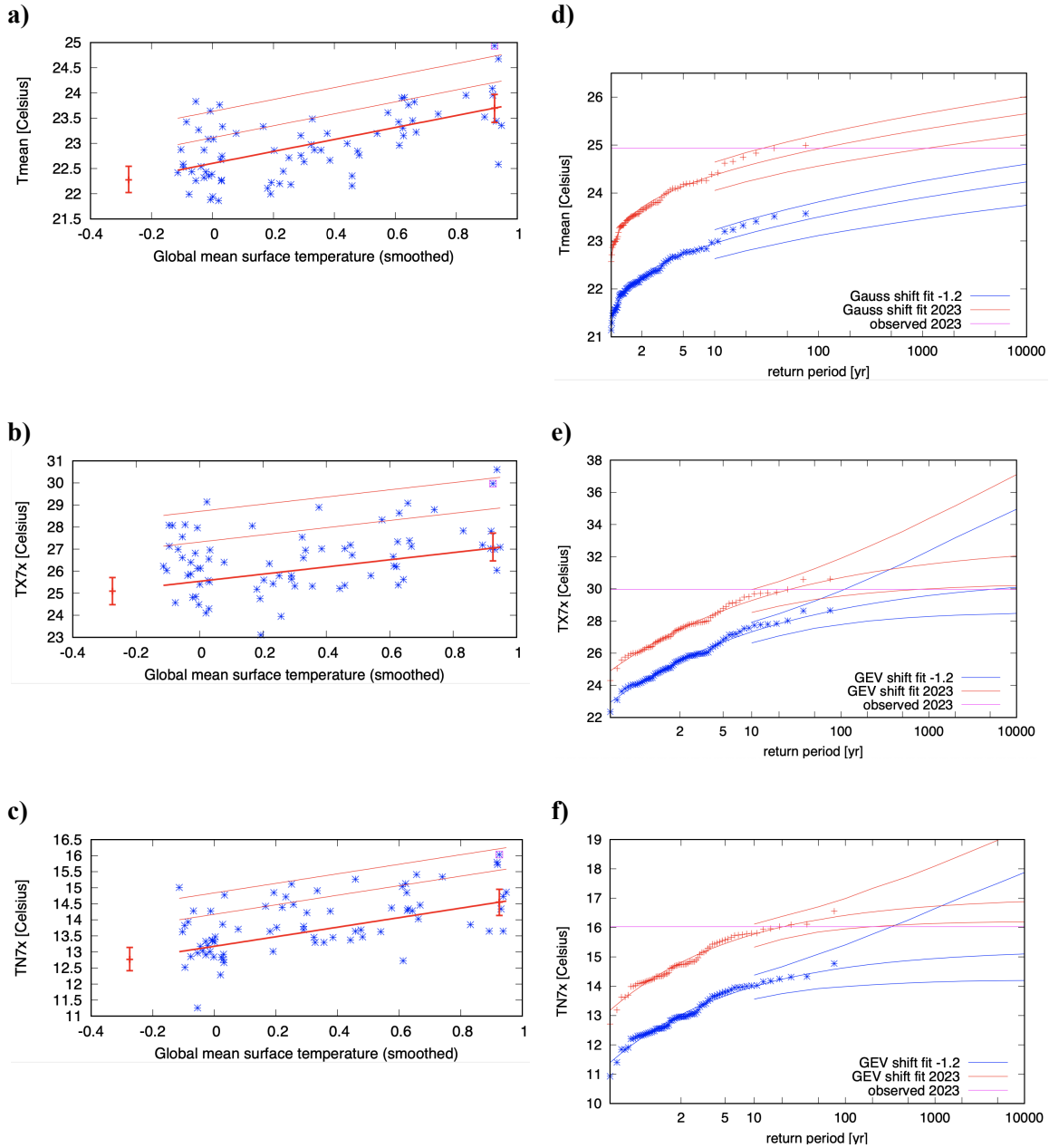
Figure 4: (**Left-hand panels** *a-c*) *October data over the study region estimated from ERA5 records to change in global mean temperature. The thick red line denotes the time-varying mean, and the thin red lines show 1 standard deviation (s.d) and 2 s.d above. The vertical red lines show the 95% confidence interval for the location parameter, for the current, 2023 climate and the hypothetical, 1.2°C cooler climate. The 2023 observation is highlighted with the magenta box.* (**Right-hand panels** *d-f*) *Return periods for the 2023 climate (red lines) and the 1.2°C cooler climate (blue lines with 95% CI), based on ERA5 data. The top panels show the results for October Tmean over Madagascar, the middle panels show the results for TX7x over Antananarivo, and the bottom panels show the results for TN7x over Antananarivo.*

3.2 Influence of modes of natural variability

Although the correlation between the ENSO cycle and temperatures is visible in October over parts of Africa, the relation between ENSO and temperatures in Madagascar is weak during October: correlations between Niño3.4-rel ([van Oldenborgh et al, 2021](#)) and temperatures over the area are around zero at this time of year (Figure 5). Nonetheless, we tested the effect of including either October Niño3.4-rel or October Indian Ocean Dipole (IOD, Figure 6) as additional covariates in the nonstationary model alongside the smoothed GMST, in an extension to the standard nonstationary model similar to that used in WWA's analysis of drought in East Africa ([Kimutai, etal 2023](#)).

A likelihood ratio test ([Neyman & Pearson, 1933](#); [Coles, 2001](#)) was used to check whether the inclusion of the extra covariate improved the fitted model enough to justify estimation of the extra parameter needed. Niño3.4-rel was not found to contribute to the fit of the linear model for any of the indices studied here. For October TX7x, the inclusion of the IOD was not found to significantly improve the model fit; for October Tmean and October TN7x, the difference between the two was found to be statistically significant. However, in preliminary analysis carried out using ERA5 data from 1950-2022 before estimates of Niño3.4-rel and IOD were available for October 2023, inclusion of the additional covariate was not found to be justified for any of the variables, suggesting that the fitted model may be rather sensitive to the inclusion of the 2023 event. Comparison of the estimated change in intensity between the GMST-only and GMST+IOD models (shown in Table 1) suggests that the contribution of the IOD covariate is relatively small, increasing temperatures by around 0.2-0.3°C for every 1°C increase in the IOD. Furthermore, the effect of including the IOD covariate on the estimated GMST trend is very small compared to the uncertainty about the trend itself: adding the IOD covariate reduces the change in intensity attributable to GMST by a little over 0.1°C. Given the dependence of the inclusion of IOD on the 2023 event, and the relative independence of the estimated trends in GMST and IOD, we therefore do not include the IOD in the final statistical model, and carry out the attribution analysis using a model that depends on GMST only.

Table 1: *Comparison of the estimated change in intensity between the GMST-only and GMST+IOD models*

	GMST-attributable change in intensity (°C)			IOD-attributable change (°C per °C)
	GMST only	**GMST + IOD**	**Difference**	
Tmean	1.424	1.317	-0.106	0.211
TX7x	1.953	1.822	-0.131	0.217
TN7x	1.784	1.615	-0.169	0.323

Figure 5: *ENSO-Temperature relationships for October, using data from ERA5. Blue colours indicate that during El Niño, temperature is below average, red colours indicate higher temperatures during El Niño. As a measure of the strength of the relationship we used the correlation coefficient with the Niño3.4-rel index.*
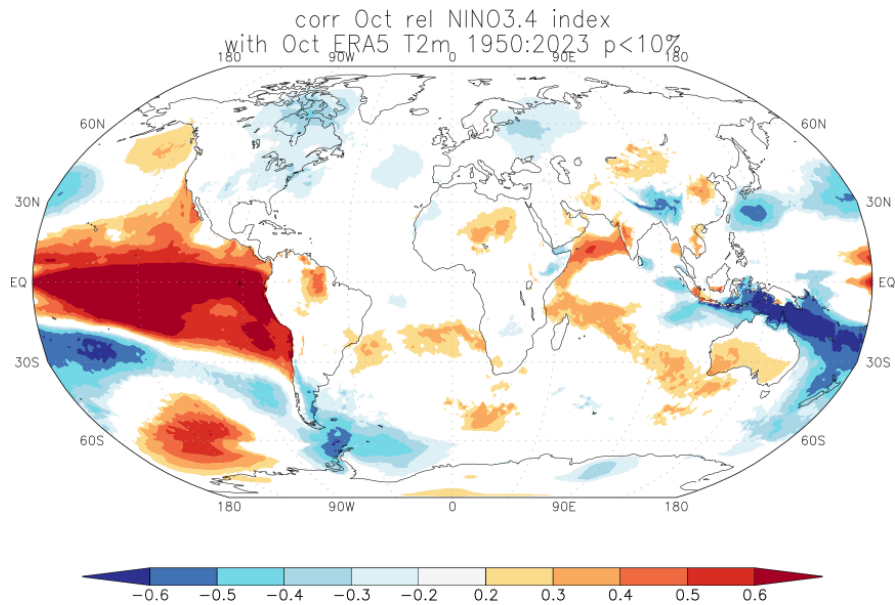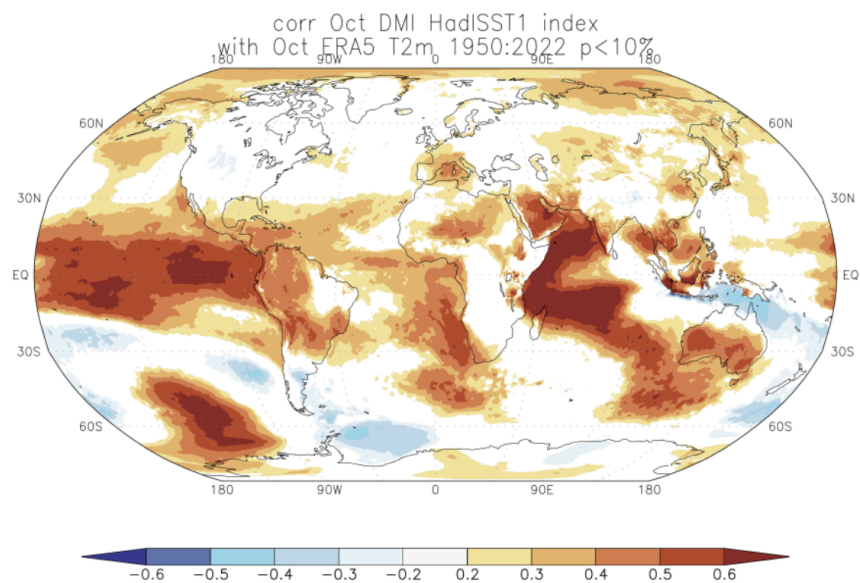

Figure 6: *IOD(DMI)-Temperature relationships for October, using data from ERA5. Blue colours indicate that during negative IOD, temperature is below average, red colours indicate higher temperatures during positive IOD.*

4 Model evaluation

In the subsections below we show the results of the model evaluation. Per multimodel ensemble (framing), WWA uses models with label 'good' as well as models that only pass the evaluation tests with one label 'reasonable'. This means that we labelled models with 'bad' if two of the tests resulted in label 'reasonable' or if the fit parameters ranges hardly overlap (see point 3. below). We exclude all 'bad' models. In addition, models for which the return period differs from observations by 5°C or more are excluded. Table 1 shows the model evaluation results. The climate models are evaluated against the observations in their ability to capture:

1. Seasonal cycles: For this, we qualitatively compare the model outputs against observations-based plots. We discard the models that exhibit multi-modality and/or ill-defined peaks in their seasonal cycles. We also discard the model if temperature seasonality varies significantly from the observations.

2. Spatial patterns: Models that do not match the observations in terms of the spatial patterns are excluded.

3. Parameters of the fitted GEV model. We discard the model if the model and observation parameters ranges do not overlap.

Table 2: *Evaluation results of the climate models considered for attribution analysis of Tmean over Madagascar domain. For each model, the expected temperature of a 1-in-100-year event is shown, along with the best estimate of the Sigma parameters and a 95% confidence interval for each, obtained via bootstrapping. The qualitative evaluation is shown in the right-hand column. Based on overall suitability, the models are classified as good, reasonable or bad, shown by green, yellow and red highlights, respectively.*

Model / Observations	Seasonal cycle	Spatial pattern	Sigma	Event magnitude [°C]	Conclusion
ERA5			0.526 (0.433 ... 0.594)	24.934 °C	
Model				**Threshold for return period 100 yr**	
ACCESS-CM2 (1)	good	good	0.679 (0.558 ... 0.751)	26.79	reasonable
ACCESS-ESM1-5 (1)	good	reasonable, pattern correlation lower than 0.8	0.684 (0.489 ... 0.831)	27.69	bad
CanESM5 (1)	good	reasonable, pattern correlation lower than 0.8	0.502 (0.401 ... 0.570)	27.01	reasonable
CMCC-ESM2 (1)	good	good	0.349 (0.270 ... 0.407)	26.04	bad
CNRM-CM6-1-HR (1)	good	good	0.613 (0.456 ... 0.747)	24.09	reasonable
CNRM-CM6-1 (1)	good	good	0.633 (0.542 ... 0.693)	24.89	bad, sigma only just reasonable

EC-Earth3 (1)	good	good	0.529 (0.391 ... 0.631)	24.85	good
EC-Earth3-Veg (1)	good	good	0.866 (0.601 ... 1.11)	25.46	bad
EC-Earth3-Veg-LR (1)	good	good	0.669 (0.540 ... 0.755)	25.22	bad, sigma only just reasonable
FGOALS-g3 (1)	good	good	0.578 (0.462 ... 0.659)	26.16	good
INM-CM4-8 (1)	good	reasonable, pattern correlation lower than 0.8	0.462 (0.363 ... 0.531)	25.87	reasonable
INM-CM5-0 (1)	good	reasonable, pattern correlation lower than 0.8	0.560 (0.449 ... 0.644)	25.76	reasonable
IPSL-CM6A-LR (1)	good	good	0.673 (0.526 ... 0.798)	24.78	bad, sigma only just reasonable
MIROC6 (1)	good	reasonable, pattern correlation lower than 0.8	0.868 (0.735 ... 0.961)	29.3	bad, high return value
MPI-ESM1-2-HR (1)	good	good	0.643 (0.501 ... 0.734)	25.53	reasonable
MPI-ESM1-2-LR (1)	good	reasonable, pattern correlation lower than 0.8	0.729 (0.562 ... 0.858)	24.68	bad, sigma only just reasonable
MRI-ESM2-0 (1)	good	good	0.567 (0.446 ... 0.659)	25.46	good
NorESM2-LM (1)	good	reasonable, pattern correlation lower than 0.8	0.444 (0.342 ... 0.508)	25.16	reasonable
NorESM2-MM (1)	good	good	0.456 (0.361 ... 0.525)	24.69	good
TaiESM1 (1)	good	good	0.450 (0.332 ... 0.527)	25.26	good
CanESM2_r1_CanRCM4 (1)	good	good	0.538 (0.434 ... 0.621)	24.278	good
HadGEM2-ES_r1_CCLM5-0-15 (1)	good	good	0.546 (0.432 ... 0.639)	23.89	good
HadGEM2-ES_r1_RegCM4-7 (1)	good	good	0.650 (0.505 ... 0.761)	26.328	reasonable
HadGEM2-ES_r1_REMO2015 (1)	good	good	0.546 (0.428 ... 0.638)	25.868	good
MPI-ESM-LR_r1_CCLM5-0-15 (1)	good	good	0.604 (0.435 ... 0.717)	23.722	reasonable
MPI-ESM-LR_r1_REMO2015 (1)	good	good	0.550 (0.399 ... 0.660)	25.549	good
MPI-ESM-MR_r1_RegCM4-7 (1)	good	good	0.851 (0.675 ... 1.00)	26.612	bad
NorESM1-M_r1_CCLM5-0-15 (1)	good	reasonable	0.372 (0.262 ... 0.456)	23.266	bad
NorESM1-M_r1_RegCM4-7 (1)	good	reasonable	0.590 (0.476 ... 0.673)	25.896	reasonable
NorESM1-M_r1_REMO2015 (1)	good	reasonable	0.439 (0.352 ... 0.503)	25.345	reasonable

Table 3: *Evaluation results of the climate models considered for attribution analysis of TX7x over Madagascar domain. For each model, the expected temperature of a 1-in-25-year event is shown, along with the best estimate of the Sigma parameters and a 95% confidence interval for each, obtained via bootstrapping. The qualitative evaluation is shown in the right-hand column.Based on overall suitability, the models are classified as good, reasonable or bad, shown by green, yellow and red highlights, respectively.*

Model / Observations	Seasonal cycle	Spatial pattern	Sigma	Shape parameter	Event magnitude [˚C]	Conclusion
ERA5			1.25 (0.939 ... 1.48)	-0.22 (-0.38 ... 0.031)	29.969	
Models					Temperature of 1-in-25 year event	
ACCESS-CM2 (1)	good	good	1.20 (0.910 ... 1.43)	-0.090 (-0.46 ... 0.15)	33.96	good
ACCESS-ESM1-5 (1)	good	reasonable, pattern correlation lower than 0.8	1.23 (0.690 ... 1.80)	-0.28 (-1.1 ... 0.37)	35.96	good
CanESM5 (1)	good	reasonable, pattern correlation lower than 0.8	1.05 (0.780 ... 1.30)	0.020 (-0.51 ... 0.26)	30.72	bad
CMCC-ESM2 (1)	good	good	1.93 (1.36 ... 2.70)	-0.62 (-1.1 ... 0.10)	30.3	bad
CNRM-CM6-1-HR (1)	good	good	1.63 (1.22 ... 1.98)	-0.20 (-0.51 ... 0.0)	31.2	reasonable
CNRM-CM6-1 (1)	good	good	1.35 (0.940 ... 1.72)	-0.21 (-1.1 ... 0.020)	27.62	good
EC-Earth3 (1)	good	good	1.07 (0.840 ... 1.33)	-0.20 (-0.80 ... 0.010)	29.08	good
EC-Earth3-Veg (1)	good	good	1.76 (1.12 ... 2.27)	-0.24 (-1.0 ... 0.29)	31.09	reasonable
EC-Earth3-Veg-LR (1)	good	good	1.38 (0.930 ... 2.08)	-0.31 (-1.1 ... 0.090)	30.12	good
FGOALS-g3 (1)	good	reasonable, pattern correlation lower than 0.8	0.700 (0.380 ... 1.02)	-0.20 (-0.97 ... 0.38)	27.87	bad
INM-CM4-8 (1)	good	reasonable, pattern correlation lower than 0.8	1.09 (0.800 ... 1.32)	-0.040 (-0.23 ... 0.23)	32.55	reasonable
INM-CM5-0 (1)	good	reasonable, pattern correlation lower than 0.8	1.05 (0.760 ... 1.30)	-0.070 (-0.27 ... 0.19)	31.95	reasonable
IPSL-CM6A-LR (1)	good	reasonable, pattern correlation lower than 0.8	1.42 (0.990 ... 1.79)	-0.32 (-0.60 ... 0.080)	26.3	reasonable
MIROC6 (1)	good	good	1.60 (1.15 ... 2.32)	-0.25 (-1.0 ... 0.080)	35.89	bad
MPI-ESM1-2-HR (1)	good	good	1.02 (0.720 ... 1.26)	-0.090 (-0.36 ... 0.28)	25.77	good
MPI-ESM1-2-LR (1)	good	reasonable, pattern correlation lower than 0.8	1.83 (1.38 ... 2.40)	-0.41 (-1.0 ... 0.19)	31.88	bad
MRI-ESM2-0 (1)	good	good	1.53 (1.02 ... 2.01)	-0.37 (-1.0 ... 0.080)	31.94	bad

Model / Observations	Seasonal cycle	Spatial pattern	Sigma	Shape parameter	Event magnitude [°C]	Conclusion
NorESM2-LM (1)	good	good	0.810 (0.570 ... 1.01)	-0.11 (-0.60 ... 0.27)	28.52	bad
NorESM2-MM (1)	good	good	1.34 (0.990 ... 1.73)	-0.070 (-0.42 ... 0.24)	31.09	good
TaiESM1 (1)	good	good	0.710 (0.510 ... 0.940)	-0.040 (-0.46 ... 0.28)	26.94	bad
CanESM2_r1_CanRCM4 (1)	good	reasonable	2.91 (2.30 ... 3.97)	-0.47 (-1.1 ... -0.25)	37.93	bad, high return value
HadGEM2-ES_r1_CCLM5-0-15 (1)	good	good	1.10 (0.870 ... 1.69)	-0.41 (-1.1 ... -0.23)	30.94	reasonable
HadGEM2-ES_r1_RegCM4-7 (1)	good	reasonable	1.21 (0.956 ... 1.66)	-0.52 (-1.2 ... -0.37)	31.33	bad
HadGEM2-ES_r1_REMO2015 (1)	good	reasonable	0.881 (0.634 ... 1.10)	-0.20 (-0.70 ... -0.0010)	31.47	bad
MPI-ESM-LR_r1_CCLM5-0-15 (1)	good	good	2.20 (1.69 ... 2.77)	-0.27 (-0.71 ... -0.023)	32.7	bad
MPI-ESM-LR_r1_REMO2015 (1)	good	reasonable	1.07 (0.808 ... 1.30)	-0.15 (-0.63 ... 0.14)	31.86	reasonable
MPI-ESM-MR_r1_RegCM4-7 (1)	good	reasonable	1.04 (0.717 ... 1.25)	-0.12 (-0.32 ... 0.18)	33.03	reasonable
NorESM1-M_r1_CCLM5-0-15 (1)	good	reasonable	1.68 (1.30 ... 2.41)	-0.55 (-1.1 ... -0.38)	32.43	bad
NorESM1-M_r1_RegCM4-7 (1)	good	reasonable	1.41 (1.08 ... 2.20)	-0.61 (-1.1 ... -0.34)	31.86	bad
NorESM1-M_r1_REMO2015 (1)	good	reasonable	1.16 (0.892 ... 1.51)	-0.22 (-0.92 ... -0.017)	33	reasonable

Table 4: *Evaluation results of the climate models considered for attribution analysis of TN7x over Madagascar domain. For each model, the expected temperature of a 1-in-20-year event is shown, along with the best estimate of the Sigma parameters and a 95% confidence interval for each, obtained via bootstrapping. The qualitative evaluation is shown in the right-hand column. Based on overall suitability, the models are classified as good, reasonable or bad, shown by green, yellow and red highlights, respectively.*

Model / Observations	Seasonal cycle	Spatial pattern	Sigma	Shape parameter	Event magnitude [°C]	Conclusion
ERA5			0.748 (0.519 ... 0.900)	-0.30 (-0.54 ... -0.0050)	16.03 °C	
Models					**Temperature of 1-in-20 year event**	
ACCESS-CM2 (1)	good	good	1.00 (0.750 ... 1.41)	-0.59 (-1.1 ... -0.38)	18.64	bad
ACCESS-ESM1-5 (1)	good	good	0.790 (0.620 ... 0.990)	-0.20 (-0.71 ... 0.05)	21.67	good
CanESM5 (1)	good	reasonable, pattern correlation lower than 0.8	0.690 (0.550 ... 0.960)	-0.28 (-1.1 ... -0.14)	22.31	bad, high return value

Model						
CMCC-ESM2 (1)	good	good	1.19 (0.970 ... 1.53)	-0.70 (-1.1 ... -0.63)	20.37	bad
CNRM-CM6-1-HR (1)	good	good	0.840 (0.610 ... 1.20)	-0.60 (-1.1 ... -0.28)	13.37	reasonable
CNRM-CM6-1 (1)	good	good	0.910 (0.730 ... 1.250)	-0.29 (-1.1 ... -0.10)	15.46	reasonable
EC-Earth3 (1)	good	good	0.910 (0.680 ... 1.27)	-0.47 (-1.10 ... -0.25)	16.32	reasonable
EC-Earth3-Veg (1)	good	good	0.810 (0.610 ... 1.00)	-0.26 (-0.76 ... -0.05)	16.54	good
EC-Earth3-Veg-LR (1)	good	good	0.900 (0.620 ... 1.36)	-0.50 (-1.12 ... -0.13)	17.48	reasonable
FGOALS-g3 (1)	good	good	0.580 (0.430 ... 0.740)	-0.33 (-1.03 ... 0.06)	20.45	good
INM-CM4-8 (1)	good	reasonable, pattern correlation lower than 0.8	0.580 (0.390 ... 0.850)	-0.49 (-1.08 ... -0.08)	22.14	bad
INM-CM5-0 (1)	good	reasonable, pattern correlation lower than 0.8	0.750 (0.570 ... 1.02)	-0.51 (-1.1 ... -0.29)	21.88	bad
IPSL-CM6A-LR (1)	good	good	0.890 (0.650 ... 1.09)	-0.21 (-0.47 ... 0.0)	17.45	good
MIROC6 (1)	good	good	0.970 (0.740 ... 1.08)	-0.55 (-0.50 ... -0.50)	20.45	bad
MPI-ESM1-2-HR (1)	good	good	0.790 (0.490 ... 1.08)	-0.27 (-1.1 ... 0.42)	16.28	good
MPI-ESM1-2-LR (1)	good	good	1.01 (0.770 ... 1.28)	-0.38 (-1.0 ... -0.22)	20.22	reasonable
MRI-ESM2-0 (1)	good	good	0.980 (0.780 ... 1.39)	-0.50 (-1.1 ... -0.35)	17.71	reasonable
NorESM2-LM (1)	good	good	0.630 (0.470 ... 0.810)	-0.27 (-1.1 ... 0.0)	19.85	bad
NorESM2-MM (1)	good	good	0.970 (0.690 ... 1.18)	-0.20 (-0.54 ... 0.020)	18.26	good
CanESM2_r1_CanRCM4 (1)	good	reasonable	0.966 (0.568 ... 1.34)	-0.28 (-1.0 ... 0.16)	14.56	bad
HadGEM2-ES_r1_CCLM5-0-15 (1)	good	good	1.30 (0.994 ... 1.94)	-0.52 (-1.1 ... -0.22)	16.8	bad
HadGEM2-ES_r1_RegCM4-7 (1)	good	reasonable	0.854 (0.647 ... 1.06)	-0.46 (-1.0 ... -0.27)	17.11	reasonable
HadGEM2-ES_r1_REMO2015 (1)	good	reasonable	0.966 (0.729 ... 1.17)	-0.28 (-0.51 ... -0.13)	17.84	bad
MPI-ESM-LR_r1_CCLM5-0-15 (1)	good	good	1.26 (0.938 ... 1.60)	-0.40 (-1.04 ... -0.14)	15.81	bad
MPI-ESM-LR_r1_REMO2015 (1)	good	reasonable	0.980 (0.753 ... 1.397)	-0.52 (-1.08 ... -0.30)	17.28	bad
MPI-ESM-MR_r1_RegCM4-7 (1)	good	reasonable	1.23 (0.896 ... 1.72)	-0.41 (-1.0 ... 0.078)	17.28	bad
NorESM1-M_r1_CCLM5-0-15 (1)	good	good	1.02 (0.751 ... 1.24)	-0.30 (-0.54 ... 0.030)	16.14	reasonable

NorESM1-M_r1_RegCM4-7 (1)	good	reasonable	1.032 (0.701 ... 1.380)	-0.27 (-1.04 ... -0.02)	17.63	bad
NorESM1-M_r1_REMO 2015 (1)	good	reasonable	0.893 (0.646 ... 1.119)	-0.39 (-0.72 ... -0.15)	17.77	reasonable

5 Multi-method multi-model attribution

This section shows Probability Ratios (PRs) and change in intensity ΔI for ERA5, CMIP6 and CORDEX models that passed evaluation.

5.1 Tmean

Model / Observations	a. Past vs. present		b. Present vs. future	
	Probability ratio PR [-]	Change in intensity ΔI [˚C]	Probability ratio PR [-]	Change in intensity ΔI [˚C]
ERA5	4.4e+4 (6.8e+2 ... 5.0e+7)	1.4 (0.93 ... 1.9)		
ACCESS-CM2 (1)	8.3e+2 (1.4e+2 ... 1.3e+4)	1.3 (0.96 ... 1.8)	15 (11 ... 26)	0.93 (0.80 ... 1.1)
CanESM5 (1)	∞ (5.0e+4 ... ∞)	1.8 (1.6 ... 2.0)	34 (17 ... 1.0e+2)	1.0 (0.95 ... 1.1)
CNRM-CM6-1-HR (1)	6.5e+2 (1.0e+2 ... 8.1e+3)	1.1 (0.79 ... 1.4)	13 (8.1 ... 26)	0.76 (0.62 ... 0.88)
EC-Earth3 (1)	4.4e+2 (93 ... 4.4e+3)	1.0 (0.80 ... 1.2)	15 (9.5 ... 32)	0.74 (0.66 ... 0.83)
FGOALS-g3 (1)	∞ (3.8e+4 ... ∞)	1.8 (1.5 ... 2.2)	33 (19 ... 77)	1.1 (0.95 ... 1.2)
INM-CM4-8 (1)	∞ (1.3e+4 ... ∞)	1.8 (1.5 ... 2.2)	25 (14 ... 63)	0.94 (0.83 ... 1.1)
INM-CM5-0 (1)	1.8e+4 (1.1e+3 ... ∞)	1.6 (1.1 ... 2.0)	19 (11 ... 45)	0.86 (0.74 ... 0.97)
MPI-ESM1-2-HR (1)	9.0e+2 (1.1e+2 ... 1.5e+4)	1.2 (0.81 ... 1.6)	15 (9.2 ... 30)	0.79 (0.66 ... 0.93)
MRI-ESM2-0 (1)	8.2e+4 (3.8e+3 ... ∞)	1.6 (1.3 ... 1.9)	28 (15 ... 67)	0.93 (0.84 ... 1.0)
NorESM2-LM (1)	1.1e+3 (1.1e+2 ... 3.1e+4)	1.0 (0.67 ... 1.4)	24 (16 ... 53)	0.87 (0.73 ... 0.99)
NorESM2-MM (1)	1.5e+4 (1.1e+3 ... ∞)	1.3 (1.0 ... 1.6)	24 (13 ... 53)	0.84 (0.72 ... 0.96)
TaiESM1 (1)	5.0e+3 (4.8e+2 ... ∞)	1.2 (0.82 ... 1.5)	26 (16 ... 59)	0.82 (0.77 ... 0.88)
CanESM2_r1_CanRCM4 (1)	1.6e+4 (2.0e+3 ... 5.0e+5)	1.4 (1.2 ... 1.6)	30 (17 ... 75)	0.84 (0.75 ... 0.93)
HadGEM2-ES_r1_CCLM5-0-15 (1)	3.3e+2 (49 ... 8.5e+3)	0.86 (0.55 ... 1.2)	13 (8.6 ... 27)	0.68 (0.59 ... 0.77)

	a. Past vs. present		b. Present vs. future	
Model / Observations	**Probability ratio PR [-]**	**Change in intensity ΔI [°C]**	**Probability ratio PR [-]**	**Change in intensity ΔI [°C]**
HadGEM2-ES_r1_RegCM4-7 (1)	4.2e+2 (37 ... 2.7e+4)	1.1 (0.70 ... 1.5)	15 (8.8 ... 38)	0.80 (0.68 ... 0.91)
HadGEM2-ES_r1_REMO2015 (1)	9.9e+2 (1.4e+2 ... 2.9e+4)	1.1 (0.77 ... 1.4)	17 (11 ... 41)	0.77 (0.66 ... 0.88)
MPI-ESM-LR_r1_CCLM5-0-15 (1)	2.8e+3 (3.5e+2 ... 1.2e+5)	1.2 (0.89 ... 1.6)	15 (8.4 ... 39)	0.72 (0.58 ... 0.85)
MPI-ESM-LR_r1_REMO2015 (1)	4.5e+4 (2.2e+3 ... 3.0e+7)	1.4 (0.97 ... 2.0)	28 (12 ... 1.4e+2)	0.80 (0.66 ... 0.96)
NorESM1-M_r1_RegCM4-7 (1)	4.2e+3 (1.6e+2 ... 1.2e+6)	1.4 (0.79 ... 2.2)	22 (12 ... 57)	0.78 (0.57 ... 0.98)
NorESM1-M_r1_REMO2015 (1)	1.7e+6 (6.7e+3 ... 7.0e+10)	1.5 (1.0 ... 2.0)	50 (24 ... 1.5e+2)	0.85 (0.69 ... 1.0)

5.2 TX7x

	a. Past vs. present		b. Present vs. future	
Model / Observations	Probability ratio PR [-]	Change in intensity ΔI [°C]	Probability ratio PR [-]	Change in intensity ΔI [°C]
ERA5	2.0e+2 (4.5 ... ∞)	2.0 (0.88 ... 3.0)		
ACCESS-CM2 (1)	44 (4.9 ... 1.0e+4)	1.6 (0.65 ... 2.4)	4.1 (3.0 ... 13)	1.3 (1.0 ... 1.6)
ACCESS-ESM1-5 (1)	1.0e+4 (0.94 ... 1.0e+4)	1.9 (1.2 ... 3.0)	5.2 (3.8 ... 29)	1.1 (0.90 ... 1.3)
CNRM-CM6-1-HR (1)	19 (1.7 ... 1.0e+4)	1.4 (0.61 ... 2.2)	2.9 (2.2 ... 6.1)	0.91 (0.59 ... 1.2)
CNRM-CM6-1 (1)	6.7 (0.40 ... 1.0e+4)	1.0 (0.22 ... 1.7)	3.4 (2.5 ... 10)	0.95 (0.69 ... 1.2)
EC-Earth3 (1)	44 (3.0 ... 1.0e+4)	1.1 (0.60 ... 1.6)	3.6 (2.7 ... 7.6)	0.95 (0.74 ... 1.1)
EC-Earth3-Veg (1)	60 (1.1 ... 1.0e+4)	1.7 (1.0 ... 2.6)	2.1 (1.6 ... 3.7)	0.80 (0.48 ... 1.1)
EC-Earth3-Veg-LR (1)	1.9e+3 (2.1 ... 1.0e+4)	1.7 (0.92 ... 2.5)	2.8 (1.8 ... 1.0e+2)	0.90 (0.54 ... 1.3)
INM-CM4-8 (1)	2.4 (0.62 ... 92)	0.84 (0.10 ... 1.6)	1.9 (1.5 ... 3.0)	0.54 (0.32 ... 0.73)
INM-CM5-0 (1)	1.5 (0.26 ... 13)	0.45 (-0.28 ... 1.3)	1.5 (1.2 ... 2.1)	0.35 (0.12 ... 0.61)

	a. Past vs. present		b. Present vs. future	
Model / Observations	Probability ratio PR [-]	Change in intensity ΔI [°C]	Probability ratio PR [-]	Change in intensity ΔI [°C]
IPSL-CM6A-LR (1)	1.0e+4 (6.8 ... 1.0e+4)	1.3 (0.65 ... 2.1)	3.6 (2.7 ... 20)	1.1 (0.92 ... 1.4)
MPI-ESM1-2-HR (1)	3.7 (0.40 ... 1.0e+4)	0.41 (-0.30 ... 1.1)	1.8 (1.3 ... 3.0)	0.48 (0.17 ... 0.81)
NorESM2-MM (1)	6.6 (1.2 ... 1.0e+4)	1.4 (0.25 ... 2.7)	2.2 (1.6 ... 3.6)	0.72 (0.40 ... 1.1)
HadGEM2-ES_r1_CCLM5-0-15 (1)	13 (2.0 ... ∞)	0.74 (0.068 ... 1.4)	2.4 (1.9 ... 3.2)	0.81 (0.54 ... 1.2)
MPI-ESM-LR_r1_REMO2015 (1)	6.0 (1.1 ... ∞)	0.96 (0.045 ... 2.1)	3.0 (2.0 ... ∞)	0.66 (0.39 ... 0.92)
MPI-ESM-MR_r1_RegCM4-7 (1)	8.0e+3 (9.4 ... ∞)	2.5 (1.3 ... 3.8)	12 (5.0 ... ∞)	1.3 (0.95 ... 1.7)
NorESM1-M_r1_REMO2015 (1)	2.8e+3 (13 ... ∞)	2.6 (1.5 ... 3.7)	7.5 (3.6 ... ∞)	1.1 (0.71 ... 1.5)

5.3 TN7x

	a. Past vs. present		b. Present vs. future	
Model / Observations	Probability ratio PR [-]	Change in intensity ΔI [°C]	Probability ratio PR [-]	Change in intensity ΔI [°C]
ERA5	∞ (12 ... ∞)	1.8 (1.1 ... 2.4)		
ACCESS-ESM1-5 (1)	92 (3.2 ... 1.0e+4)	1.6 (1.1 ... 2.1)	4.8 (3.4 ... 8.5)	0.95 (0.78 ... 1.1)
CNRM-CM6-1-HR (1)	1.0e+4 (0.093 ... 1.0e+4)	0.66 (0.24 ... 1.1)	5.5 (4.3 ... 15)	0.80 (0.63 ... 0.93)
CNRM-CM6-1 (1)	10 (0.073 ... 1.0e+4)	1.0 (0.54 ... 1.4)	3.8 (2.8 ... 6.0)	0.77 (0.59 ... 0.91)
EC-Earth3 (1)	1.0e+4 (66 ... 1.0e+4)	1.1 (0.75 ... 1.5)	5.7 (4.0 ... 14)	0.85 (0.67 ... 0.99)
EC-Earth3-Veg (1)	3.6e+2 (2.3 ... 1.0e+4)	1.3 (0.95 ... 1.7)	4.1 (3.0 ... 8.2)	0.76 (0.61 ... 0.91)
EC-Earth3-Veg-LR (1)	1.0e+4 (96 ... 1.0e+4)	1.9 (1.5 ... 2.4)	7.4 (5.4 ... 14)	1.1 (0.97 ... 1.3)
FGOALS-g3 (1)	1.0e+4 (4.1 ... 1.0e+4)	2.1 (1.8 ... 2.4)	12 (8.4 ... 30)	1.3 (1.1 ... 1.4)
IPSL-CM6A-LR (1)	6.0 (0.58 ... 1.0e+4)	0.41 (-0.030 ... 0.82)	3.3 (2.5 ... 5.1)	0.55 (0.40 ... 0.68)
MPI-ESM1-2-HR (1)	1.0e+4 (4.7 ... 1.0e+4)	1.0 (0.65 ... 1.4)	5.2 (3.7 ... 10)	0.72 (0.55 ... 0.91)
MPI-ESM1-2-LR (1)	1.0e+4 (1.0e+4 ... 1.0e+4)	0.97 (0.30 ... 1.7)	3.9 (2.5 ... 8.6)	0.83 (0.51 ... 1.1)

Model / Observations	a. Past vs. present		b. Present vs. future	
	Probability ratio PR [-]	Change in intensity ΔI [˚C]	Probability ratio PR [-]	Change in intensity ΔI [˚C]
MRI-ESM2-0 (1)	1.0e+4 (15 ... 1.0e+4)	1.9 (1.3 ... 2.5)	5.6 (4.2 ... 11)	0.98 (0.79 ... 1.2)
NorESM2-MM (1)	2.2e+2 (2.7 ... 1.0e+4)	1.3 (0.55 ... 2.0)	3.1 (2.1 ... 4.9)	0.69 (0.45 ... 0.93)
HadGEM2-ES_r1_RegCM4-7 (1)	∞ (22 ... ∞)	0.80 (0.36 ... 1.3)	3.6 (2.9 ... 6.3)	0.62 (0.44 ... 0.79)
NorESM1-M_r1_CCLM5-0-15 (1)	2.5 (0.42 ... ∞)	0.41 (-0.36 ... 1.2)	2.2 (1.5 ... 3.9)	0.47 (0.22 ... 0.72)
NorESM1-M_r1_REMO2015 (1)	∞ (2.7e+6 ... ∞)	2.1 (1.1 ... 2.8)	13 (5.2 ... ∞)	0.85 (0.59 ... 1.1)

6 Hazard synthesis

For the event definitions described above we evaluate the influence of anthropogenic climate change on the events by calculating the probability ratio as well as the change in intensity using observations and climate models. Models that do not pass the evaluation tests described above are excluded from the analysis. The aim is to synthesise results from models that pass the evaluation along with the observations-based products, to give an overarching attribution statement. Figs. 7-12 show the changes in probability and intensity for the observations (blue) and models (red). To combine them into a synthesised assessment, a term to account for intermodel spread is added (in quadrature) to the natural variability of the models. This is shown in the figures as white boxes around the light red bars. The dark red bar shows the model average, consisting of a weighted mean using the (uncorrelated) uncertainties due to natural variability plus the term representing intermodel spread (i.e., the inverse square of the white bars). Observation-based products and models are combined into a single result in two ways. Firstly, we neglect common model uncertainties beyond the intermodel spread that is depicted by the model average, and compute the weighted average of models (dark red bar) and observations (dark blue bar): this is indicated by the magenta bar. As, due to common model uncertainties, model uncertainty can be larger than the intermodel spread, secondly, we also show the more conservative estimate of an unweighted, direct average of observations (dark red bar) and models (dark blue bar) contributing 50% each, indicated by the white box around the magenta bar in the synthesis figures.
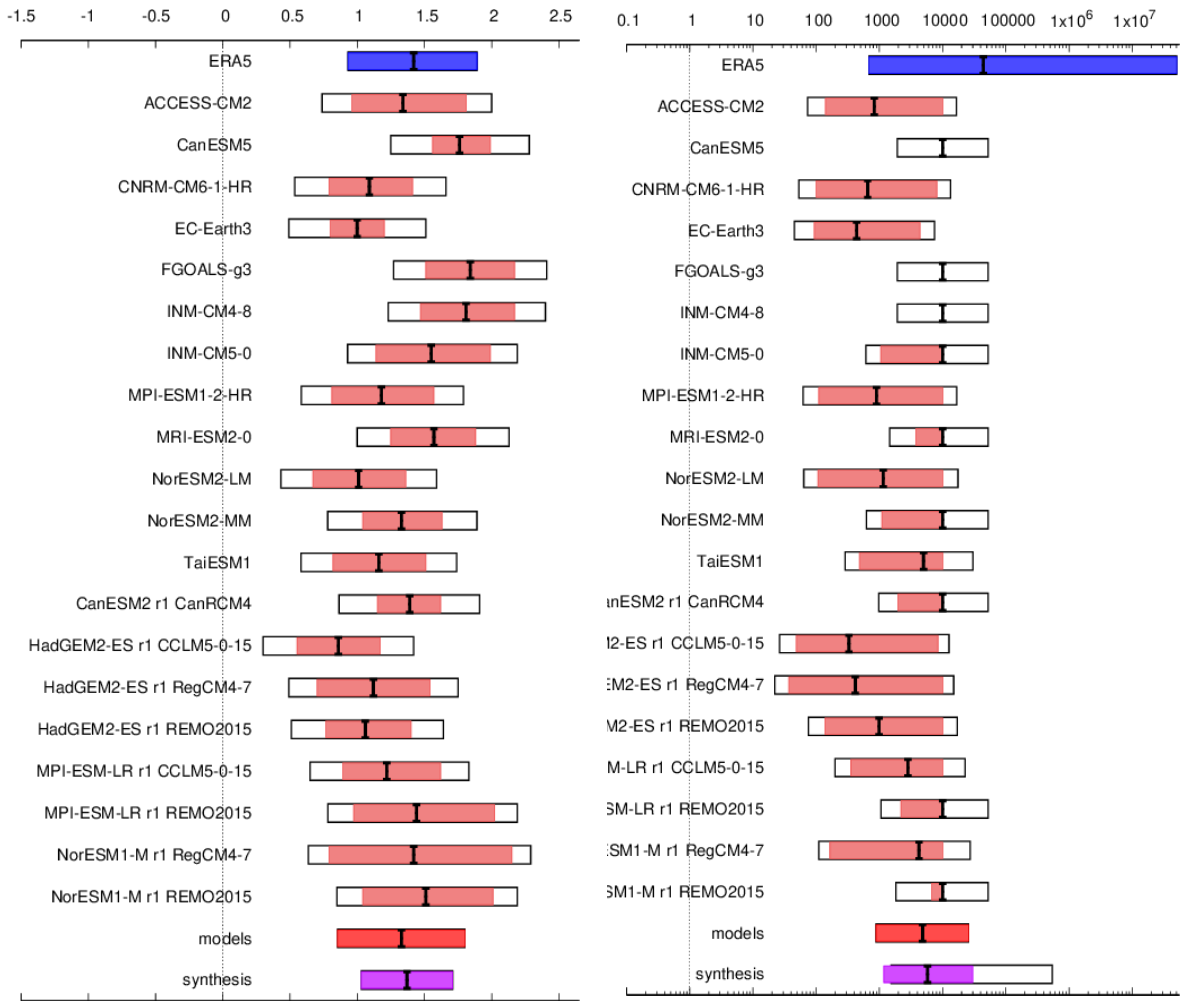
Figure 7: *Synthesis of intensity change (left) and probability ratios (right), when comparing the October Tmean event over Madagascar with a 1.2C cooler climate.*
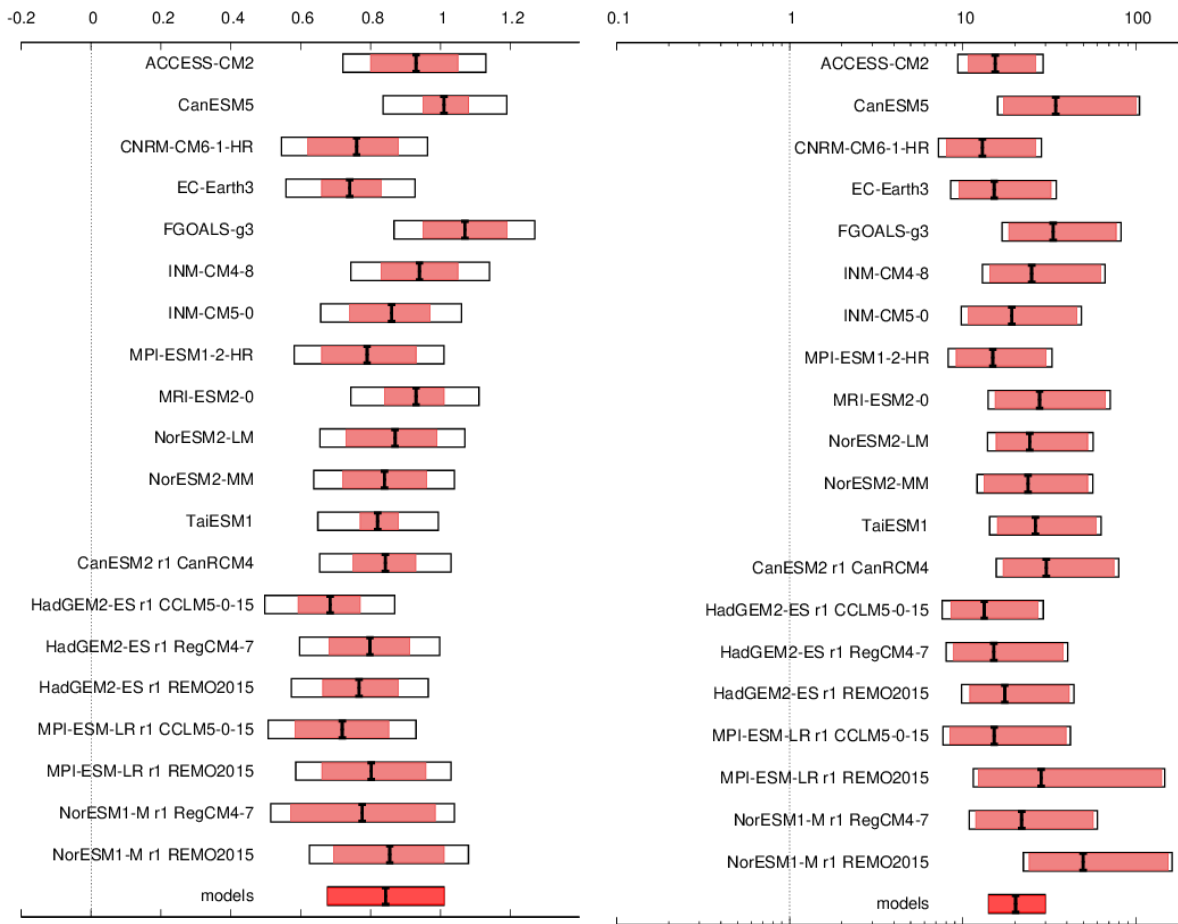
Figure 8: *Synthesis of intensity change (left) and probability ratios (right), when comparing the October Tmean event over Madagascar at 0.8°C warmer (2°C since pre-industrial) climate and the current climate*
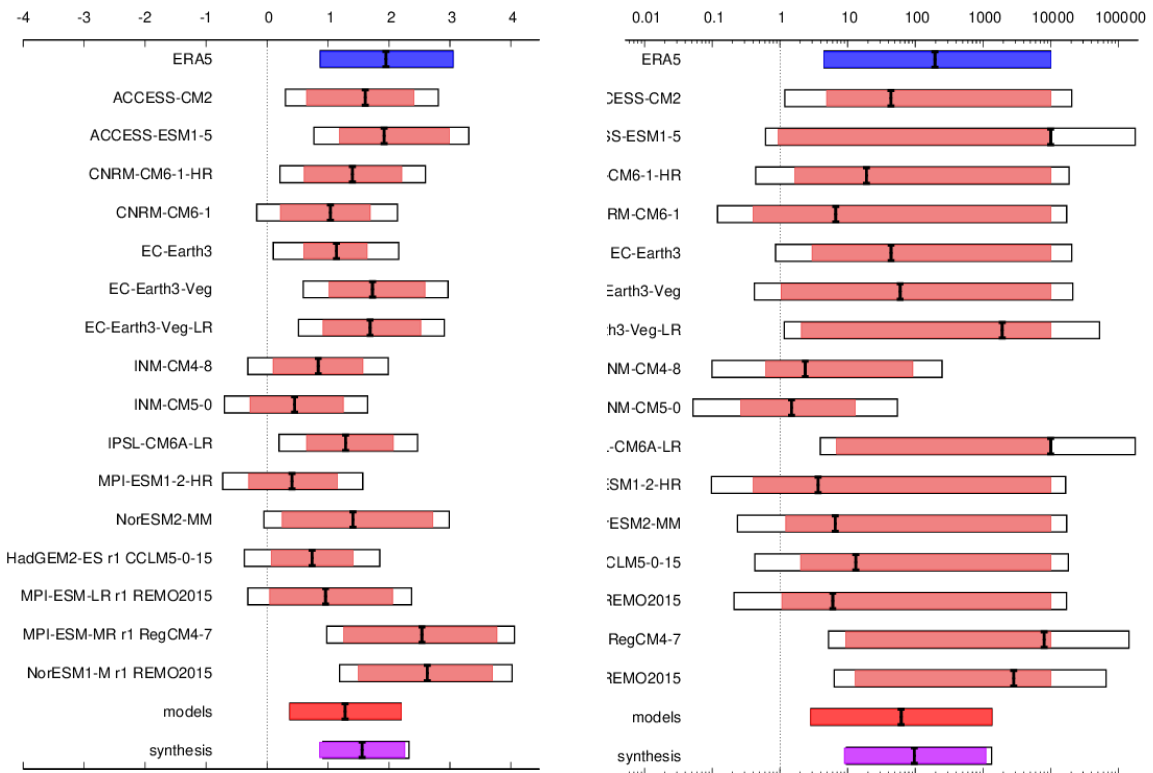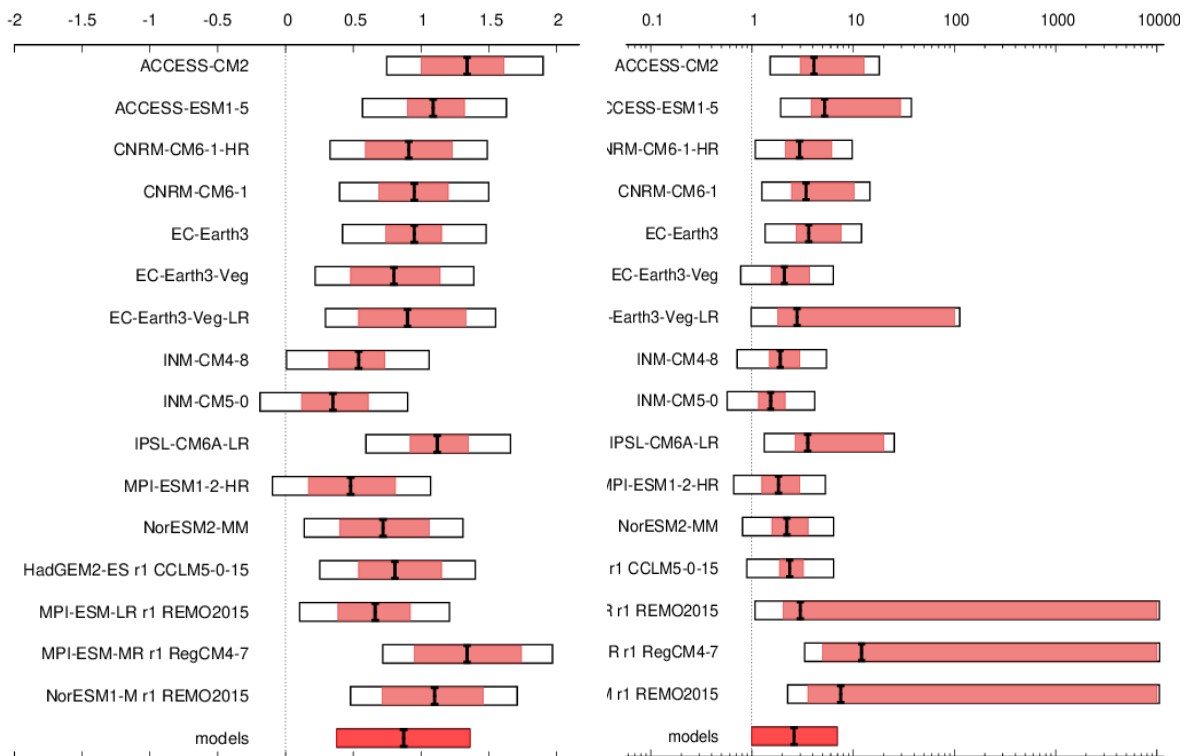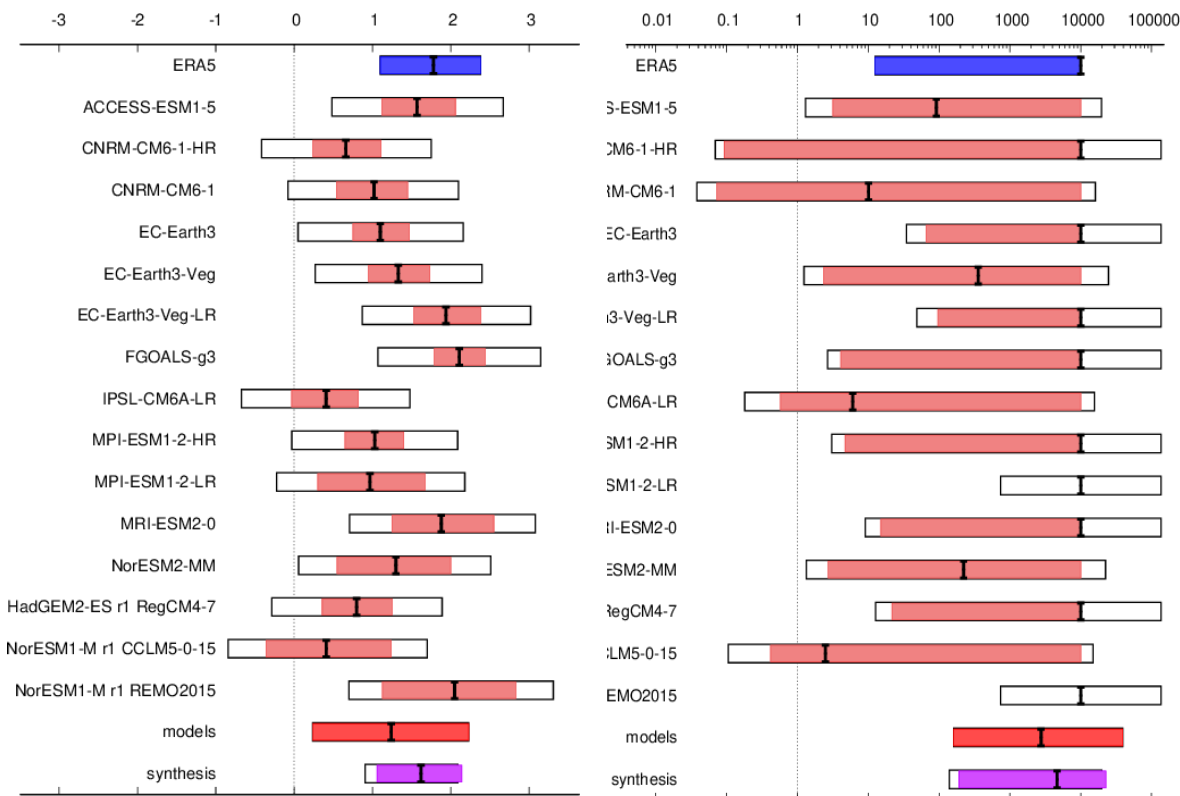
Figure 9: *Synthesis of intensity change (left) and probability ratios (right), when comparing the October TX7day event over Antananarivo with a 1.2C cooler climate.*
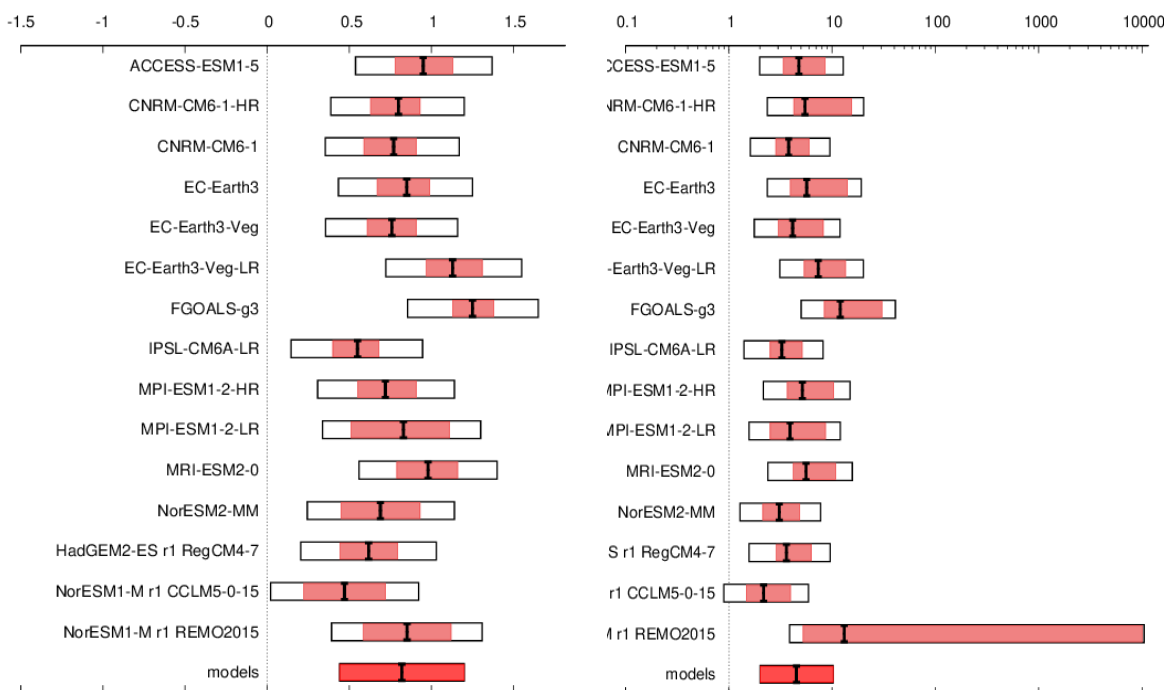

Figure 10: *Synthesis of intensity change (left) and probability ratios (right), when comparing the October TX7day event over Antananarivo at 0.8°C warmer (2°C since pre-industrial) climate and the current climate*

Figure 11: *Synthesis of intensity change (left) and probability ratios (right), when comparing the October Tn7day event over Antananarivo with a 1.2C cooler climate.*

Figure 12: *Synthesis of intensity change (left) and probability ratios (right), when comparing the October Tn7day event over Antananarivo at 0.8°C warmer (2°C since pre-industrial) climate and the current climate*

Due to very large or infinite values in probability ratios between the present and the past, the synthesised probability ratio is not well defined. This is because any quantification requires "infinity" to be replaced with a real number, and the choice of this arbitrary number influences not only the upper but also the lower bounds and the best estimate, even when the best estimate and lower bounds are finite for all datasets. We also emphasise that when synthesised probability ratios are large (and likely much larger than 100), exact values are no longer meaningful. We therefore do not report the change in likelihood of the past to present climate, but only give a lower bound with a high confidence in the qualitative conclusion that there is a strong trend, but a low confidence on the exact number. For all other measures (probability ratios for future-present and intensity changes) we report the weighted averages and note that the differences to the unweighted are minimal.

For Tmean over Madagascar the intensity change between the present and the past is 1.37°C (1.03 to 1.71°C). For a future 2°C warmer climate, models indicate an increase in intensity of another 0.843°C (0.677 to 1.01°C). The synthesis of probability ratios indicates a very large increase between the present and the past 1.2°C cooler climate, that is larger than 100. Towards a future 2°C warmer climate, models indicate a further factor increase of 20.2 (14.1 to 29.9).

For TX7x over Antananarivo the intensity change between the present and the past is 1.56°C (0.865 to 2.26°C). For a future 2°C warmer climate, models indicate an increase in intensity of another 0.871°C (0.380 to 1.36°C). The synthesis of probability ratios indicates a very large increase between the present and the past 1.2 cooler climate that is larger than 10. Towards a future 2°C warmer climate, models indicate a further factor increase of 2.60 (1.00 to 6.92).

For TN7x over Antananarivo the intensity change between the present and the past is 1.62°C (1.06 to 2.14°C). For a future 2°C warmer climate, models indicate an increase in intensity of another 0.820°C (0.442 to 1.20°C). The synthesis of probability ratios indicates a very large increase between the present and the past 1.2°C cooler climate that is larger than 100. Towards a future, 2°C climate models indicate a further factor increase of 4.51 (2.01 to 10.2).

The results for all three event definitions are combined in the summary findings as an intensity change of between 1 and 2°C for the intensity change up till now and we state that the events have been made more than 100 times more likely in case of the October mean and 7-day Tmin temperatures and more than 10 times more likely in the case of the 7-day Tmax. We emphasise that these numbers given for probability ratio are the lower bounds and that the best estimates are much higher. The 7-day Tmin and Tmax definitions both relate to the same heat event. Whilst TX7x showed lower factor changes of at least 10 in likelihood, the TN7x showed changes so large that we are confident that such an event as experienced this year would not have occurred without human-induced climate change. We reflect this by choosing the wording "would not have occurred without human-induced climate change" in the title of the study. Changes in a 2°C warmer world are summarised by stating that none of these events would be rare at that warming level. Due to the lines of evidence discussed above and many other studies on heat extreme coming to similar conclusions, confidence is high in the high level results and intensity changes.

7 Vulnerability and exposure

Extended periods of high temperatures or heat waves can have negative consequences for many aspects of human society including agriculture, human health, and even lead to an increase in heat-related fatalities. The number of people exposed to heat waves between 2000 and 2016 has increased by around 125 million (WHO, 2018). The western Indian Ocean southeast of Madagascar recorded marine heat waves as early as May 2023 (Copernicus, 2023), even before WMO declared the onset of El Nino in July 2023. Inhabitants in the southern and southwestern regions of the island are facing escalating challenges with worsening water scarcity and famine related to multiple factors (Hending and Holdereid, 2023), including climate variability and deforestation which are only expected to worsen as climate change continues (Hending et al., 2022).

Temperatures in some regions of Madagascar rose to 40 °C in October 2023 and continued up to a week, putting residents and ecosystems under pressure, raising concerns about the health of citizens, and with potential repercussions on the country's agriculture and biodiversity (Fleuria, 2023). Similar temperature conditions were seen in Madagascar during another episode of intense heat waves in 2019 (Météo Madagascar, 2019) which were extremely impactful on children, with consequences like malnutrition, diarrhea, and dehydration (Linfo.re, 2019). Like in many parts of Africa, there is limited research and real-time reporting on heat risk and heat-related impacts in Madagascar, and therefore it's difficult to quantify the particular impacts of this episode. However, research on extreme heat impacts in places similar to Madagascar can be extended, along with knowledge and data on vulnerability to describe the likely impacts of extreme heat in this region.

7.1 Intersecting vulnerabilities

The climate in Madagascar, including extreme weather events, can impact production activities, elevating the risk of geographic poverty, climate-induced poverty, and regression into poverty. Heat exposure in Madagascar has been linked to lost economic potential with GDP being negatively influenced by higher temperatures, probably due to lost productivity in climate sensitive sectors such as agriculture, which accounts for 30% of the country's GDP and employs large parts of the population (Andrianady et al., 2023). It is estimated that 1,610 million hours of labour have been lost in 2022 due to heat exposure in the agricultural, construction, manufacturing and service industry alone in Madagascar (Romanello et al., 2023). Like other disasters, elevated temperatures can also heighten the susceptibility to poverty among vulnerable groups due to many intersecting vulnerabilities (Alcantara-Ayala et al, 2023; Raju, Boyd and Otto, 2022; Li et al., 2022). Parts of Madagascar have been through a major drought recently (Harrington et al, 2023). The drought impacts combined with the ongoing heat wave can make living conditions worse. Another longer-term impact from warming temperatures includes an increasing prevalence and range of mosquitoes, contributing to the rise in malaria cases in Antananarivo (BMZ, 2021).

Anticipated rises in temperature extremes carry significant consequences for humanity, especially in the African continent, home to some of the world's poorest and most vulnerable populations (Asefi-Najafabady et al., 2017). Madagascar is the world's fourth most at-risk country to climate change (USAID, 2023). The INFORM Risk Index score for Madagascar is currently at 5.5, with a 7.1 score for the 'lack of coping capacity' indicator, indicating limited infrastructure and institutional capacity to cope (DRMKC, 2023) with different hazards, including heat waves. Disasters worsen impacts on food security and malnutrition, especially impacting subsistence farmers. Chronic malnutrition is already prevalent at 42%, and there is the potential for further escalation due to the repercussions of the COVID-19 pandemic. As one of Africa's nations prone to disasters and food

insecurity, Madagascar currently faces a critical situation. Almost 2 million individuals in the country are grappling with severe hunger, requiring urgent humanitarian aid. In the southern regions, the driest conditions in four decades have compelled the population to resort to unconventional sources such as locusts, raw red cactus fruits, and wild leaves for sustenance (WFP, 2023). In regions marked by persistent vulnerabilities, household sizes often exceed the national average and this exacerbates precarious living conditions.

7.2 Informality and urban planning

Madagascar is mostly rural, with 61% of people living in rural areas. However, the country is experiencing high urbanisation rates, with a 4.5% increase per year resulting in an urban population of 7 million in 2018, compared to 2.8 million in 1993 (African Development Bank, 2019; UN Habitat, n.d.-a). Due to this unprecedented urban growth, informal housing settlements have emerged in larger as well as smaller urban pockets and can be expected to increase without adequate urban planning country wide (World Bank, 2020). Hence, informality is a key concern in Madagascar, given that these conditions could lead to exacerbated impacts (Raju, Boyd and Otto, 2022) during disasters such as the ongoing extreme heat events as experienced in October 2023. While informal housing might occur in rural as well as urban areas, informality exacerbates heat exposure and risk especially in densely populated areas of cities due to formation of Urban Heat Islands (UHI). To our best knowledge no studies on UHI exist in Madagascar, but studies from other low-income African countries show UHI cluster around densely populated areas and informal settlements due to close proximity of buildings and reflecting building materials (Gyimah, 2023; Li et al., 2021; Walle et al., 2022). Data collected from 13 cities in Madagascar on building materials of "traditional buildings", shopping centres, restaurants, administrative buildings, schools and hospitals shows that traditional buildings, mostly found in informal settlements, are constructed mainly of metal sheets across all study sites, indicating a high potential for UHI due to the exacerbating heat effect of metal sheets (Nematchoua et al., 2020). Further, thermal comfort was assessed, revealing the lowest comfort hours related to heat in hospitals with only 5.1% of yearly comfort hours, followed by traditional buildings. Hence vulnerability is exacerbated for patients potentially arriving at overheated hospitals as well as health staff working under intense conditions, although clear evidence is missing in the literature particularly for the African context (Nyembwe, 2023). Geographically, Antsiranana and Tulear had the most discomfort hours related to heat and are located in the transition tropical and arid tropical climates (Nematchoua et al., 2020).

While, generally, poverty levels in rural areas are nearly twice as high as in urban areas (45% compared to 88%), urban poverty is increasing at an alarming rate across all urban areas leaving large parts of the population in vulnerable positions (World Bank, 2023). Antananarivo as the capital has experienced significant unplanned growth, leading to increased urban poverty. In fact, the city has had the highest national poverty rate of all cities closing in on 66% based on last updated numbers in 2012 (UN Habitat, n.d.-b). High poverty coincides with peak population density as much as 2000 inhabitants/built hectares in central areas, 8 times higher than the Greater Antananarivo region (Ramiaramanana and Teller, 2021). Therefore, poverty, dense population, potentially higher heat exposure are likely drivers contributing to severe disaster impacts. Furthermore, while migration towards cities is often driven by economic incentives, the majority of jobs in urban areas are in the informal economy, leaving large parts of the population in vulnerable living and working conditions, exposed to heat (IOM UN Migration, 2019). Extreme heat might drive migration in the first place through either direct or indirect pathways e.g connected to livelihood in rural areas, yet migrating populations face urban poverty and precarious housing situations related to heat vulnerability,

resulting in a reinforcing feedback loop (Issa et al., 2023). The large informal sector is concentrated in the garment manufacturing sector and trade predominantly located in rural areas, and work is usually executed either from home or without specific premises (Afavi et al., 2023). This population group is therefore particularly vulnerable to heat waves as the majority of the activities involved are being carried out under unsafe conditions, potentially outside, and in roughly 90% of the cases without access to water in both (Afavi et al., 2023).

To cope with extensive heat exposure, hydration and access to cool places are crucial (CDC, 2022). Yet, the vast majority of Madagascan households (73%) in both urban and rural areas lack access to on-site drinking water, and 45% use surface- or other unimproved water sources for drinking (UNICEF, 2019). Consequently, in 2018, approximately 66% and 49% of the rural and urban population were deprived of drinking water, respectively, being at risk of dehydration and infection from water borne diseases (USAID, 2021). Seeking cooler spaces might be challenging for urban populations. Urban green spaces offer natural cooling spots while reducing UHI simultaneously, while the absence of urban green spaces exacerbates UHI significantly (Walle et al., 2022). To the best of our knowledge, no data on urban green spaces is available for Madagascar. Regardless, of all public buildings compared, hospitals show the lowest cooling energy consumption, and highest discomfort during heat, leaving particularly vulnerable groups such as children and elderly at increased risk of premature death and cardiovascular complications (Nematchoua et al., 2020; Schlüter et al., 2020 Phung et al., 2016).

To cope with increasing heat stress and other challenges arising from rapid urbanisation, urban planning needs to incorporate heat adaptation plans and consider migration influxes. According to the UN Economic Commission for Africa, as of 2015, only 16% cities had developed urban plans and the influx and socioeconomic challenges with increasing migration towards urban areas have not been considered by local governments and cities in the planning process (UNECA, 2015; European Commission, 2021). However, from 2019 IOM cooperates with relevant stakeholders at national and local levels to support integration of migration in urban development planning. First guidelines are already being tested in Madagascar as well as in Ecuador and Nepal (European Commission, 2021). Furthermore, the Agence Française de Development (AFD) supports three projects as part of the PADEVE project in urban development focusing on sanitation, climate change and improvement of living conditions (Centre for Affordable Housing Finance Africa, 2021).

7.3 Health systems, electricity, and WaSH

The population share affected by at least one heat wave per year in Madagascar is projected to rise from 0.2 % in 2000 to 4.8 % in 2080. This is related to 24 more very hot days per year over this period. As a consequence, heat-related mortality is estimated to increase by a factor of four by 2080 (GIZ, 2021). However, more than 60% of the population in Madagascar resides over 5 kilometers away from a healthcare facility, frequently in remote and challenging-to-access regions lacking proper infrastructure such as roads and communication networks. Among children, risk of dying is one of the highest in the hot seasons (Schluter et al., 2020). The distribution of health personnel is uneven, and certain areas face the risk of running out of essential drugs and medical supplies, leading to unavailability (USAID, n.d.). As climate change increases the likelihood of encountering heat waves and the urgent nature of the situation, emergency departments and healthcare systems should implement procedures for promptly identifying and addressing heatstroke (Rublee et al., 2021). Additionally, access to health care might be limited, e.g in Ambalavao only two health centres staffed with at least one medical doctor exist, for a population of 45,000, whereas access in rural areas is even

more limited, as two thirds of the rural population live at least 5 km away from a primary health care facility (European Commission, 2021; Garchitorena t al., 2021).

It is estimated that no more than 25-33% of the population has access to electricity (International Energy Agency, 2022; World Bank, 2023), while only 15% of rural communities are connected to Madagascar's national energy grid (EIB, 2023). To reduce this rural energy poverty, in November 2020, Power Africa and USAID made a US$1.2 million investment in developing mini-grids to deliver sustainable energy to 1,500 households across villages in central Madagascar (ShareAmerica, 2023). Reinforcing this approach, in January 2023 the European Investment Bank, Triodos Investment Management, and EDFI ElectriFI announced a €19 million investment in WeLight Madagascar's €28 million project to build and develop solar mini-grids across another 120 rural communities; ensuring clean and affordable energy to more than 45,000 households and businesses (EIB, 2023). Further, a few months later, in April 2023, the World Bank approved a US$400 million credit for the Digital and Energy Connectivity for Inclusion in Madagascar Project, which endeavors to double energy access from 33.7% to 67% in Madagascar, targeting 150 currently underserved villages (World Bank, 2023).

Access to electricity is one of the critical ways of deploying active cooling strategies in times of extreme heat, e.g. fans are useful and safe at indoor temperatures reaching up to 39C (Jay et al., 2021). While it is not known to what extent the following cooling and coping strategies were deployed during the heat wave of focus and previous heat spells, there are effective risk reducing measures for individuals that do not require electricity, including behavioral changes (such as drinking more water and visiting cooling centres), installing shade on exterior surfaces and windows, and water immersion and taking showers (Jay et al., 2021). Said strategies in turn highlight the urgency of access to water, sanitation and hygiene (WASH) services. However, only roughly half of the population has access to basic water services - a figure which is closer to 36% in rural contexts (UNICEF, n.d.) - while only 12.3% have access to basic sanitation services (World Bank, 2022). In fact, in south Madagascar, only 4.2 percent have access to a quality water supply from an improved water source (Fayad, 2023). The widespread lack of both electricity and WASH services thus compound the heat risk faced by Malagasy people. Night-time temperatures remain high, as they did throughout October, and the lack of relief from heat exposure is increasingly recognized to significantly aggravate heat-related mortality and morbidity. Research by He et al. (2022) on 28 cities across Japan, China, and South Korea suggests that relative mortality risk can rise by up to 50% on days with hot nights compared to days without. Similarly, Murage et al. (2017) find that, in England, hot nights can pose greater danger than high day-time temperatures, notably to patients with chronic ischemic diseases and stroke. This is particularly alarming in the context of our study, as our findings confirm the vast increase in likelihood of high minimum temperatures.

To improve the quality and access of basic WASH services across Antananarivo and five secondary cities, the Government of Madagascar and World Bank jointly launched the National Water Project in June 2022, investing over US$220 million (World Bank, 2022). The project seeks to enhance WASH services for 115,000 students, connect 460,000 of the poorest and most vulnerable households to the national water and sanitation networks while supporting another 165.000 households, and boost the climate-smart reconstruction of water systems after the several cyclones which hit the island in 2022, improving the water infrastructure's resilience to not only storms and floods but also drought. In December 2022, USAID made a US$30 million investment to improve access to safe water and sanitation in rural eastern Madagascar (US Embassy Antananarivo, 2022), helping 225,000 people gain access to drinking water and 625,000 people to sanitation services (Global Waters, 2022). With the highest extreme poverty rate in the world, at 91% of the population, and one of the world's lowest

child survival rates globally, of which one-quarter of fatalities are linked to water, said investments will be critical to addressing Madagascar's high vulnerability to climate hazards like heat waves.

7.4 Heat action planning, preparedness, and response

The National Meteorological Services of Madagascar, Météo Madagascar, provides forecasts for high temperatures. For example, on October 19, 39 °C was forecasted for that day and the day after in parts of Madagascar (Météo Madagascar, 2023a; Météo Madagascar, 2023b; Météo Madagascar, 2023c). However, while no functional heat early warning system is in place over Madagascar, including formal heat wave criteria and advisories, the national disaster office has a framework for crafting impact-based forecasts and disseminating warning messaging for floods, cyclones, and other storms via mass media and mobile phones that instruct recipients on measures to take to reduce risks (IFRC, 2020; WMO, 2023). Without adaptation, Madagascar is estimated to be facing a fourfold increase in heat-related mortality per 100,000 people over the coming decades (BMZ, 2021), which highlights the importance of existing early warning systems to expand to also encompass extreme heat, along with investments in adaptation.

Lastly, similarly to most countries on the African continent, Madagascar currently does not have a Heat Action Plan (HAP) or equivalent protocols for managing heat risk. In the coming years, it will be increasingly important to develop a heat early warning system and corresponding plans, in order to build local capacity and preparedness for heat.

7.5 V&E conclusions

Overall, Madagascar remains highly vulnerable to the types of extreme heat that have been found to be increasing in intensity and frequency in this study. This is particularly true for areas that already suffer from chronic food insecurity, such as the very southern part of Madagascar where drought conditions and extreme poverty combine with high temperatures to create negative impacts to human health and wellbeing. In addition, the very high poverty rates in the country, combined with limited coverage and access to health systems, electricity, and WASH services means that most individual and household cooling and coping strategies are inaccessible. A high degree of informal settlements and unplanned urbanisation leave large parts of the population particularly exposed to high temperatures. Together the loss of productivity/income for agricultural sectors, precarious housing situation, urban poverty, large workforce in informal economies intersect to worsen impacts of heat waves. While Madagascar currently lacks heat action plans and a comprehensive early warning system, and has limited formal preparedness for heat waves, these are key gaps that can be filled to reduce impacts in the future.

Data availability

Almost all data are available via the Climate Explorer.

References

All references are given as hyperlinks in the text.
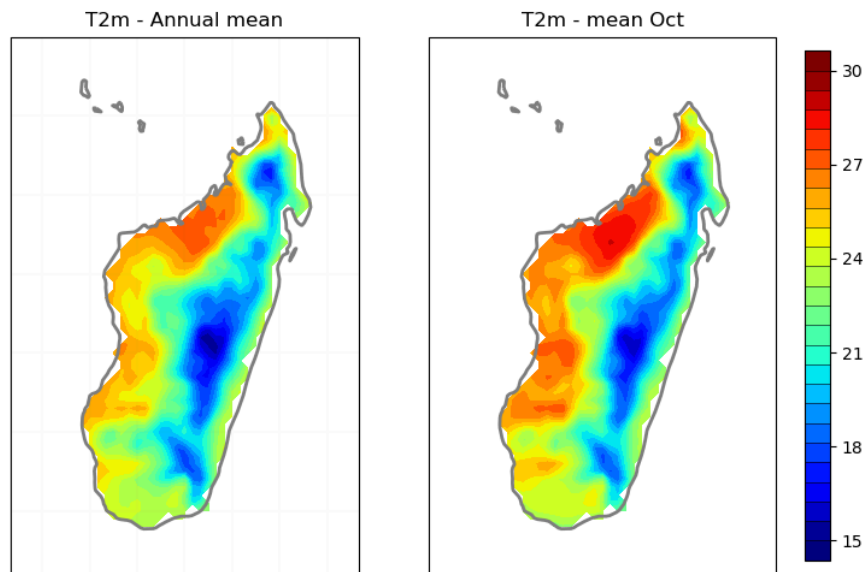
Supplementary figures

Figure S1: *T2m climatological annual (left) and October (right) means. Data from ERA5 for the period of 1980-2023 (Units: degree C).*